Universidad Carlos III

The assessment of the different magnetic field topologies found in plasma propulsion thrusters using a finite element code.

Author: Maria Acuña Moncayo

Tutor: Pablo Fajardo

Bachelor's Degree in Aerospace Engineering

September 2015

Acknowledgements

First of all, I would like to express my sincere gratitude to my advisor Dr. Pablo Fajardo for the continuous support, for his patience in every moment, motivation, and knowledge. He guided me and he helped me in all the time of research and writing of the present project.

My sincere thanks also goes to the EP2 group as they provided me all the needed information they had in order to perform this thesis. Without they precious support it would not be possible to conduct this research.

Also, I would like to thanks my colleagues during this four years as they allow me to discover and think about to many issues. And moreover, they make this experience really satisfactory, without them it would have been incomplete.

Last but not the least, I would like to thank my family for supporting me throughout writing this thesis and in my life in general.

Abstract

Electrical thrusters can be used as a useful alternative to the chemical thrusters, the major dominant in the spacecraft industry due to their high specific impulse, and thus low fuel consumption, which results in smaller fuel weight.

The Hall Effect Thruster is included in the electrostatic category as the plasma is formed inside the chamber of the thruster. It is based of electrons thrown into a chamber from an external cathode towards an inner anode, inducing an axial electrostatic potential an ionizing the injected neutral gas. A magnetic field is also induced, in order to prevent electrons from reaching the anode too quickly and also accelerate the ionized heavy particles that will generate thrust.

On the other hand, the Helicon Plasma Thruster could be considered as an interesting alternative based on the energy source energy in the form of Helicon Plasma Sources. From the point of view of the energy, the HPT behaves as an electrothermal thruster, heating the plasma with RF waves radiated from an antenna and supersonically expanding it in a magnetic nozzle. From the thrust generation point of view, the HPT behaves as an electromagnetic thruster, due to the interaction between the azimuthal plasma currents during the supersonic expansion and the magnetic field lines, that produces an action-reaction force that accelerates the plasma and confers thrust to the vehicle.

This bachelor thesis is focused on the analysis of the influence of the different magnetic elements (such as solenoids, coils or even permanent magnets, etc. used in the design of the magnetic circuits of both thrusters) on the magnetic field topology.

To perform the study, an open-source, finite-element method code is used. This code allows to calculate the magnetic field of different magnetic circuits to evaluate their influence.

In the case of the Hall thruster, the different parameters to get the desire magnetic element configuration and intensity have to been developed by trial and error configuration.

On the other hand, in the case of the HPT, actual information implemented in a prototype performed by EP2 and Sener is used. In a first approximation, punctual elements are taken into consideration, and in further analysis filling factor are included so as to add more realism to the model.

Contents

List of Figures

List of Tables

Chapter 1

Introduction and scope

This chapter will provide the reader with context for the development of this project, in order to be able to understand the fundamentals of the magnetic field of the electric propulsion, specially the Helicon Plasma Thruster (HPT) and the Hall Effect Thruster, the two thrusters dealt with during this project.
The main objectives and sections of the present project will also be discussed in this chapter, after the background of the electric propulsion has been explained.

1.1 Electric Propulsion

In the field of space propulsion, chemical thrusters had always been the major dominant due to the lack of sufficient electrical power supply of the early equipment.
As the research in the electric propulsion field advanced, some important advantages of the electric propulsion systems with respect to the chemical one were found (explained at 1.1.2).
The main advantage of these propulsion systems [1] is that they are more fuel-efficient than chemical thrusters, although they deliver less thrust. This is the reason why their range of operability is restricted to space missions.
Considering the definition of the EP thruster (thruster that makes use of the electrical thruster to achieve higher exhaust velocities and thrust), this propulsion systems can be divided into electrothermal, electrostatic and electromagnetic acceleration.

- Electrothermal acceleration: the fundamental working principle of this category is to heat a fluid or gas that is injected into the thruster chamber via electric power, and afterwards the heat flow is expanded and accelerated in a nozzle, converting the deposited thermal energy into axial energy, yielding thrust. The specific impulses obtained are linked to the system used and the maximum temperature achieved. Within this kind of thrusters, there are two main exponents are: Resistojet and ArcJet. In the case of the Resistojet thruster, the injected flow is heated via a resistor across which a certain voltage is applied, the values obtained are 150-200 s. On the other hand, Arcjet thruster uses a cathode-anode couple with a high voltage, and an electric arc is created heating the flow. The values obtained are 280-1500 s.

- Electrostatic acceleration: plasma flow is created inside the thruster chamber (typically achieved through electron bombardment, which ionizes the neutral gas upon collisions), and a cathode-anode couple induces a strong electrostatic potential in the axial direction in order to accelerate the ions. The specific impulses obtained are between 2500 and 7000 s.

- Electromagnetic acceleration: the acceleration of ions is achieved by exploiting the interaction effects between an applied or self-induced magnetic field with the electron currents and/or the electric field. Within this category the Hall Effect Thrusters are going to be included. The specific impulse of this kind of thruster are of the order of 1500 and 3000 s.

For the prototype models there is no actual regulations in which they can be comprehend. This projected is focused on the elaboration of these models, so there is no applicable regulations withing the present thesis.

1.1.1 State of the art

From the moment in which electric propulsion started to be a new possible of manner of propulsion systems in the aerospace field, researches on this topic suffers interest changes depending on the historical moment.
It was not until the 1960s, when the researches were looking for obtaining high power with low weights, when the first space Electric Propulsion (EP) thrusters were ready to be tested in flight. For such a reason, they had experience a great development ever since. During the 1970s, the enthusiasm with this way of obtaining thrust decayed, and consequently the study of these motors decreased too. But, during Cold War, scientific researches focus on plasma motors (Hall Effect) and at the end of the 1980s, they tested and realized more than fifty missions with this kind of propulsion systems. At the end of the Cold War, all these researches, carried out by private companies, tried to make profits of this kind of propulsion, what implied an increase of interest on this type of propulsion systems.
In a Joint Propulsion Conference [6] took place in California, it was announced that the American corporation Boeing practiced a successful experience with the 702HP product line of hybrid chemical/electric propulsion satellites. Consequently, they developed the 702SP products -an all electric propulsion satellites what implies an new increased of interest in this kind of propulsion.

1.1.2 Technology Justification

The analysis of the justification of the electrical propulsion compared to the chemical will be based on thrust and specific impulse.

$$F = \dot{m} u_e \tag{1.1}$$

$$I_{sp} = \frac{F}{\dot{m}_{prop} g_0} = \frac{\dot{m} u_e}{\dot{m}_{prop} g_0} = \frac{u_e}{g_0} \tag{1.2}$$

where $\dot{m}_{prop}$ is the mass flow of the propellant and $\dot{m}$ stand for the mass flow leaving the thruster; u_e is the effective exhaust velocity and g_0 is the gravity constant at standard sea level.
In order to obtain thrust, some mass flow is spent and accelerated by different means, in order to achieve the greatest value of exhaust velocity, and consequently a greater value of thrust.
In the case of chemical thrusters, they make use of the combustion reaction between a gas and oxygen to heat the mass flow, and implement thermal energy into it. Then, the resulting hot gas expands, and the thermal internal energy derived from combustion is converted into axial kinetic energy, accelerating the gas particles and achieving the highest possible exhaust velocity. These processes have some limitations regarding the maximum temperature that could be achieved in the combustion chamber and the expansion that can take place in the nozzle region. Those are mainly related to the maximum operating temperature of the materials used in the chamber and the size of the nozzle. Moreover, there is a limitation on amount of energy per unit mass of the propellant, higher mass flow implies higher thrust but the fuel consumption is also higher.
In the case of EP thrusters, there are several principles to achieve acceleration of the mass flow particles: electrothermal, electrostatic and electromagnetic acceleration (previously described) with which the exhaust

velocities can be around an order of magnitude higher, according to some the valuable information. This yields specific impulses with a higher order of magnitude, meaning that EP thrusters operate in a more efficient way in terms of propellant utilization. At the same time, the thrust obtained is considerably lower than in the chemical thrusters because of the smaller mass flow dealt with in these thrusters.
The difference in the order of magnitude between the thrusters has important implications. In order to show them, the classic ideal Tsiolkovsky rocket equation (see [2] for further information) is going to be regarded:

$$\frac{m_{final}}{m_{initial}} = exp\left(-\frac{\Delta V}{u_e}\right) = exp\left(-\frac{\Delta V}{I_{sp}g_0}\right) \tag{1.3}$$

where $m_{initial}$ and m_{final} are, respectively, the total mass of our vehicle at the beginning and at the end of the mission, and ΔV is the change in velocity required to perform an orbit maneuver from a certain trajectory to another.
This lies one of the main advantages of the EP with respect to the chemical propulsion. The exponential factor affects the amount of payload carried for a mission. For an acceptable payload level, u_e must be comparable to the required V. Therefore, the usage of EP is useful for long range missions with large ΔV, while chemical thrusters would led to an small amount of payload for this type of missions. As previously said, the thrust in the EP thrusters is small, leading to a long missions, which is not a problem as time is not a limited factor in most cases in space missions.
Another application for the electric thrusters is to maintain a determined orbit. This is important as spacecraft's trajectories, small deviation can occur needed to be corrected. In order to do so, small amount of thrust could be employed, and consequently, EP should be used. This grants an easier control, and a more exact orbit correction.
On the other hand, the main drawbacks of the electric propulsion is related to the limitation of the range of operability, totally restricted to space missions. Moreover, the small amount of thrust deliver makes the mission takes longer.
During the present project, Hall Effect Thruster and Helicon Plasma Thruster are going to be the selected ones to be treated.

1.1.3 Operation principle of Hall Effect Thruster

One of the thruster that this project deals with is the Hall Effect Thruster [4], also called Stationary Plasma Thruster (SPT). It is characterize by its geometry mainly axisymmetric and it is compounded by electromagnets and/or permanent magnets surrounding the chamber; a exterior cathode that radiates electrons and an inner anode that receives and canalizes some of the electrons from the cathode; and a feeding system (see Figure 1.1).
The functioning of these thrusters are similar to the rest of EP thrusters. It is based on the ionization of a gas (produced by the collisions of the electrons and neutral atoms) and it is accelerated thanks to a electric field created through the difference in voltage between the cathode and the anode. A radial magnetic field is also applied, in order to prevent electrons from reaching the anode too quickly and ensure the existence of a adequate ionization region. Finally, the cathode ejects the necessary electrons in order to neutralize the ions that are accelerated out of the chamber.

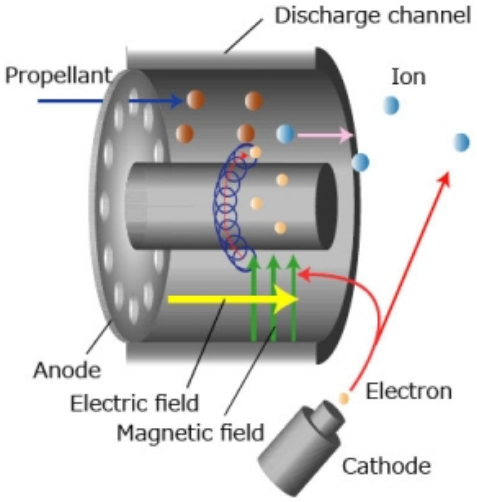

Figure 1.1: Scheme of the Hall Effect Thruster. Source University of Tokyo, Hall Thruster Research Group

1.1.4 Operating principle of to Helicon Plasma Thruster

The other thruster assessed within this project is a different type of EP thrusters: the Helicon Plasma Thruster (HPT) [3]. The basic functioning and differences with respect to the previous thrusters are going to be briefly discussed hereinafter.

Helicon plasma thrusters derived from the study of Helicon Plasma Sources, as it was found a frequency range - whistler waves - that produces ionization on a gas column inducing the plasma state. As a thruster, the HPT has a relatively simple and cheap design. They are characterized by high plasma densities and good thrust performance for high compactness.

The main components of this thruster are a cylindrical chamber where the plasma is produced. A radio-frequency (RF) antenna wrapped around the chamber, whose power is supplied thanks to the RF subsystem consisting on a power unit a wave generator/amplifier, and a matching network. A feeding system attached to the back of the chamber and several electromagnets and /or magnets surrounding the chamber. Those lasts elements are going to be studied during the complete present project. Regarding the processes involved, the emission and propagation of the wave from the antenna to the plasma; the absorption of the RF wave energy (deposited mainly on the electrons); these electrons bombard the neutral gas (producing high density plasma) and the generated plasma is guided by the magnetic field are the most relevant ones.

The attractiveness of these devices is that, in comparison with other electric propulsion devices, they do not need any electrode, grids or neutralizers, leading to simpler and more robust devices, with a long lifetime due to the limited plasma-wall interaction.

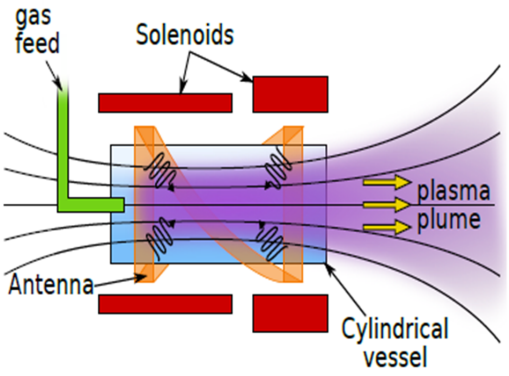

Figure 1.2: Scheme of the HPT [5]

Summarizing, the HPT achieves thrust with the combination of electrothermal and electromagnetic acceleration of the plasma. On one hand, plasma is heated inside the chamber and expanded after the thruster; and on the other hand, the electrons currents interact with the magnetic field lines.

1.1.5 Activities performed by the EP2 group

The EP2 group (Equipo de Propulsion Espacial y Plasma) focused on the studies related to the electric propulsion systems [7]. This group was started at the Universidad Politecnica de Madrid and in 2013 it was moved towards Universidad Carlos III de Madrid.
During this years of working, they had developed relevant advanced in the electric propulsion field. For example, there is a cluster working on the H2020 (one of the researches projects by the European Union).
For each kind of thruster, they are concentrated on the physical behavior taking place. This allows to develop mathematical models and simulation codes to explain the iteration of all the physical phenomena and the influence of the different control parameters.
In the frame of HET, the activity of EP2 is focused on the theoretical study and simulation of thrusters with different plasma propulsion systems. The most relevant results achieved by EP2 are:

1. The first complete fluid code of the chamber.
2. Detail models of the iteration between the plasma and the wall chambers.
3. Second and later versions of the hybrid HPHall code, originally created at Space Propulsion Laboratory (SPL) - MIT.
4. Double stage thruster models with intermediate electrodes.

Within this field, the present project deals with the behavior of the magnetic field when control parameters of the magnetic circuit are changed. Notice that plasma iterations are out of the scope of this project.
Another branch is related to the Helicon Plasma Thruster. In this case, EP2 have some agreements with Sener company and they are both interest in these thrusters and the magnetic nozzles of them. The project began in 2008 as a part of the European project HPH.com to design and develop a mini-HPT. The studies are related to:

- Internal development of the plasma inside the chamber.
- Plasma acceleration in the exterior magnetic nozzle and its separation. The convergent-divergent nozzles are able to guide, expand and accelerate the plasma.

- The formation of discontinuities inside the plasma in some conditions.

Nowadays, one of the main activities of investigation related to HPT is devoted to the study of the plasma downstream with respect to the magnetic field that forms the nozzle, once the fluid has been accelerated. Within this topic the project could be included, but not been focus just on the nozzle region, but also in the chamber.
The present project is of importance for the design of HPT, in particular, for the design of its magnetic circuits. Several studies have been developed to analyze the effect of the magnetic circuit on the magnetic topology.

1.2 Objectives of this project

The main objective of this project is the analysis of two important thrusters within the electric thrusters category, the Hall principle motor and the Helicon Plasma Thruster. Several tasks towards the main one are going to be listed:

1. Understand the fundamentals of the finite element for magnetostatic computations and the program used during the complete project, in particular the FEMM code that will be described in section 2.2.

2. Understand the different magnetic elements that form each of the thruster, its function and its location within the thruster.

3. Analyze the most relevant parameters of the magnetic elements and studied their influence chamber magnetic topology and the magnetic nozzle.

1.3 Structure of this document

In this section a brief summary of the contents that will be covered in this document are described. This gives an idea of the planing of the work followed during the duration of the project.
This first chapter has presented the key points of EP technology, the operating principles of HET and HTP and the objectives to be pursued during the project.
Chapter 2 describes the main concepts of the finite element method within the magnetostatic computations. Moreover the basics concepts of the code used during the present project, FEMM 4.2. are also described. It also deals with some characteristics of the magnetic field found in the HET and one of the elements treated, the solenoids.
Chapter 3 describes the method used to as to obtain the magnetic field topology of the thruster implemented as well as different studies related to the magnetic elements used and different topologies of other thrusters.
Chapter 4 shows the magnetic field topology of the HPT used by the EP2 group with the Sener Company. Moreover, studies related to magnetic elements used are been performed.
Chapter 5 presents the budget used in order to perform the present project.
Chapter 6 details the conclusions of the project as well as further projects that could be performed.

Chapter 2

Finite Element Method

In this chapter, the reader will understand the basis of the Finite Element Method (FEM) as well as a brief description of the code used in order to solve the different magnetic configurations implemented hereinafter. Moreover, some characteristics of the magnetic elements will be explained too.

2.1 Introduction to Finite Element Method

The concept of the Finite Element Method had been used for centuries. Some examples of these uses could be found with the Egyptians, people who used this method to calculate the volume of the pyramids, or even the Chinese mathematician, Lui Hui, who employed a 3072 side regular polygon to calculate the length of circumference in order to get an approximation of the number π.
The method, as it is known nowadays, is mainly related to the structural calculations in the aerospace field. In the 40's, Courant proposed the use of polynomic functions to solve the deformation field in elastic problems. After that, Turner, Clough, Martin and Topp introduced in their work, the application of finite element to the analysis of aeronautical structures using discretized and shape function concepts.
From that point on, and related to the evolution of computers, the method followed a continuous evolution until it gained the importance that it has nowadays as procedure to solve magnetic field problems.
The partial differential equations arise in the mathematical modelling of physical phenomena and diverse subject areas such as fluid dynamics, electromagnetism - the one of interest in the present project - material science, astrophysics... It is not always possible to find an analytical solution for those systems. For such a reason, FEM techniques are implemented in order to solve those partial differential equations in a wide range of engineering problems. FEM allows to obtain a the solution of a system in a easier and more economic way than a prototype. However, it has to be kept in mind, that FEM gives an approximate solution. Errors come from the mathematical model and the integration and resolution of the equations themselves, therefore prototypes are still necessary.
The main idea is to transform a continuous system (infinity degrees of freedom) governed by a differential equation to a system with a finite number of degrees of freedom represented by a system of algebraic equations.
In every FEM problem, some common elements can be found:

- Domain. Geometric space where the system is going to be analyzed.
- Boundary conditions. They are known and they are relevant to the solution problem.
- Unknowns. They are the variables that are needed to be solved.

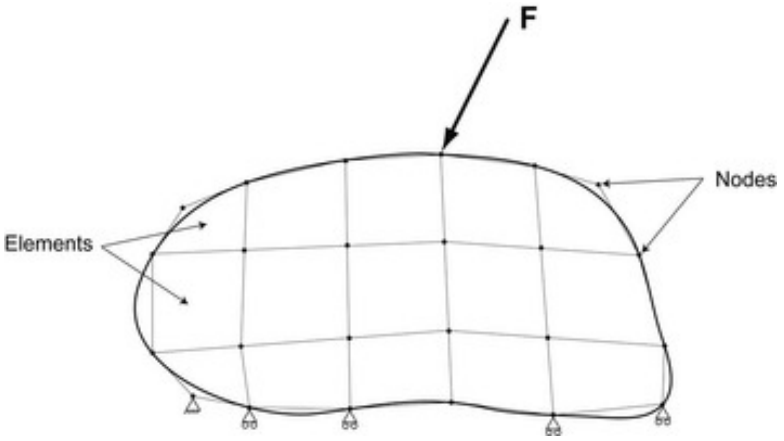

Figure 2.1: Schematic illustration of a finite element model[19]

In order to solve the problem, the following steps are taken into consideration:

- The computational domain is shaped and sized subdomains defined by means of lines, surfaces or volumes. Those subdivisions are called elements and the main restrictions are related to the overlapping of elements and the complete cover of the whole domain. The behavior of the elements is specified in some limited parameters related to the nodes - grid points located on the union point of elements-.
- The unknown variables are then set at the different nodes of the problem. They are called degrees of freedom of the model.
- Then, a set a functions that define the variation of the unknown variables in each element with respect to their value at at the node are defined. Those functions are known as shape or interpolating functions.

So, FEM is, basically, a method that allows to compute the unknowns variables of an engineering problem by means of problem discretization.
The main advantages of the use of FEM are related to the possibility of handle a lot of different engineering problems. It permits to assess the performance and safety previous to the manufacture process, identify and solve problems earlier,... These solutions depend on the number of elements uses, the higher the elements, more accurate the solution is.

2.2 FEMM 4.2 Code

The program that will be used during this thesis is FEMM 4.2. It its a open source (and thus free licensed) code which allows to calculate some limiting cases of Maxwell's equations (see [8] for further information). It addresses magnetic problems in which displacement currents can be ignored. In a similar vein, the electrostatics takes into consideration cases in which only the electric field is important, and the magnetic might be neglected. Moreover, FEMM solves 2D/axysymmetric steady-state heat conduction problems.
The one of interest during this project is the magnetic problem. The magnetic fields considered and time invariants and obey the following equations:

$$\nabla \times (H) = (J) \tag{2.1}$$

$$\nabla \cdot (B) = 0 \tag{2.2}$$

where the B is the flux density, H is the field intensity and J is the current density, and the relation between the first two is:

$$(B) = \mu(H) \tag{2.3}$$

where μ is the permeability.
If the material is nonlinear, the permeability is a function of $B(H)$. Then equation 2.3 can be expressed as:

$$\mu = \frac{(B)}{(H)(B)} \tag{2.4}$$

In order to satisfy equations 2.1-2.4, the program finds a magnetic field by means of a magnetic vector potential approach; so the flux density is rewritten in terms of the vector potential A.

$$B = \nabla \times A \tag{2.5}$$

Then,

$$\nabla \times \left(\frac{1}{\mu(B)} \nabla \times (A) \right) = J \tag{2.6}$$

For a linear isotropic material (and assuming $\nabla \cdot A = 0$), equation 2.6 reduces to:

$$-\frac{1}{\mu} \nabla^2 (A) = (J) \tag{2.7}$$

To deal with a nonlinear problem, FEMM retains equation 2.5 and the magnetostatic problem is solved.
In the general 3-D case, A is a vector with three components. However, in the 2-D planar and axisymmetric cases, two of these three components are zero, leaving just the component in the "out of the page" direction. The advantage of using the vector potential formulation is that all the conditions to be satisfied have been combined into a single equation. If A is found, B and H can then be deduced by differentiating A. The form of equation 2.6, an elliptic partial differential equation, arises in the study of many different types of engineering phenomena.
To solve the problem, boundary conditions need to be established. The different options when using FEMM are:

- Dirichlet. The value of potential A is explicitly defined on the boundary i.e. $A = 0$ along a boundary to avoid magnetic flux from boundary.
- Neumann. The normal derivative of potential along the boundary is specified. For example, in magnetic problems, $\frac{\partial A}{\partial n} = 0$ is defined along a boundary to force flux to pass the boundary at exactly a 90° angle to the boundary.
- Robin. It a sort of mix between Dirichlet and Neumann, giving a value of A and its derivative at the boundary. For example, $\frac{\partial A}{\partial n} + cA = 0$.
- Periodic. It joins two boundaries together. In this type of boundaries, the values on the corresponding points of the two boundaries are set equal to one another.
- Antiperiodic. It also joins two boundaries, but the boundary values are made to be of equal magnitude but opposite sign.

If no boundary conditions are explicitly defined, each boundary defaults to a homogeneous Neumann boundary condition. However, a non-derivative boundary condition must be defined somewhere in order to have a unique

solution.
For axisymmetric magnetic problems, $A = 0$ is enforced on the line $r = 0$. In this case, a valid solution can be obtained without explicitly defining any boundary conditions, as long as part of the boundary of the problem lies along $r = 0$.
Once all the parameters of the problems have been set, Finite Element Method is applied to obtain a solution. The discretization of the domain in FEMM is done using triangular elements. Over each element, the solution is approximated by a linear interpolation of the values of potential at the three vertices of the triangle.
The linear algebra problem is formed by minimizing a measure of the error between the exact differential equation and the approximate differential equation as written in terms of the linear trial functions.
The magnetic field solved during this thesis are axisymmetric. Moreover, zero frequencies problem will be selected, meaning that the problem dealt with is DC one.
One of the main advantages of this program is that it can be linked to Matlab. This permits to obtain graphics, images, solutions in an easier and more easy to handle way, and could eventually allow to implement optimization algorithms in Matlab. This was the first task to be developed during the project. In order to make this connection between programs, some commands must be implemented in Matlab (see [9] for commands information).

2.3 Magnetic circuits. Elements

2.3.1 Axisymmetric magnetic field

The problems dealt with during this thesis are going to be axisymmetric problems, and although the problem is treat as it was, in the Hall Effect Thruster, the real circuit could not be implemented axisymmetric because outer solenoids are placed in a discrete position surrounding the chamber of the thruster.
For that purpose, the reluctance parameter will be used. It is analogous to the resistance in an electrical circuit but it stores magnetic energy. According to [10], the reluctance $\mathbb{R} = \oint \frac{dl}{\mu A}$ for a simplified scheme of the magnetic circuit could be estimated:

$$\mathbb{R}_h \sim \frac{l_h}{\mu_h S} \tag{2.8}$$

and

$$\mathbb{R}_\delta \sim \frac{l_\delta}{\mu_\delta S} \tag{2.9}$$

where $\mathbb{R}_h$, $\mathbb{R}_\delta$, l_h, l_δ, μ_h, μ_δ are the reluctance, longitudes and permeability associated to the magnetic core (h) and the air gap (δ). Assuming that the material in the air gap is vacuum $\mu_h/\mu : \delta \sim 10^3$ and $l_h/l_\delta \sim 10$, it results in:

$$\frac{\mathbb{R}_h}{\mathbb{R}_\delta} \sim 0.01 \Rightarrow \mathbb{R}_h << \mathbb{R}_\delta \tag{2.10}$$

In this way, it could be demonstrated that the magnetic core is the one that allows the magnetic flow and the air gap is the one that needs the greater magneto-motive force. As the air gap is axisymmetric, it might be assume that the magnetic field generated by it might also be.

Solenoids VS Permanent Magnets elements

The use of solenoids to magnetic excitation in Hall Effect Thrusters and Helicon Plasma Thruster is really logic as they allow to have the control of the magnetic field in all the moments. The problem starts with the appearance of the minithrusters because they need higher magnetic field intensity and some inconveniences

related to volume, power dissipated begin to appeared. For that reason, permanent magnet utilization is needed. In the case of the solenoids, given the intensity of the magnetic field B, the current have the expression shown at 2.11.

$$B \sim \mu_\delta \frac{NI}{\delta} \tag{2.11}$$

where μ_δ is the permeability, N is the number of turn and δ is the air gap distance and I is the current. So, the B α L^{-1} or B α P_d^{-1} where L is the length of the chamber and P_d is the power of the thruster. Once the side and power of the thruster are been reduced, the magnetic field may be increased and to do so, either intensity or volume of the solenoids must be increased.

Every solenoid, getting used of Equation 2.11, and according to Gallardo and Parra [11] have the following expression for the power dissipated:

$$P_{mag} = R \cdot I^2 \sim \frac{(\delta B))^2}{L} \sim \frac{\delta^2}{L^3} \tag{2.12}$$

Due to the small differences of the gap air in this kind of thrusters the power to be dissipated increases when the size of the thruster is decreased.

In space vehicles, the refrigeration is performed by means of heat conduction and/or radiation. This type does of refrigeration does not able to dissipate the huge amount of hear realased. For that reason, the use of permanent magnets could be beneficial in order to reduce the electric power consumed by the thruster in order to generate the magnetic field.

2.3.2 Magnetic field intensity

From equation 2.11, it could be found that the relation between the magnetic field and the intensity of the solenoid is linear (see Figure 2.2).

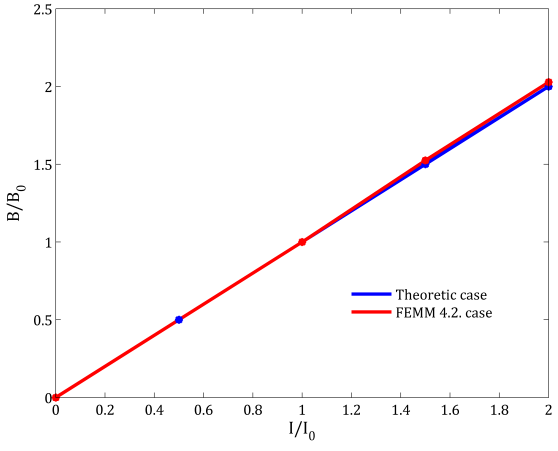

Figure 2.2: Evolution of the intensity of the magnetic field as a function of the intensity.

Figure 2.2 is obtained with the initial reference of the Hall Effect Thruster (see 3.1).

This analysis allows to validate the theoretical approximation once it had been compared with the results obtained with FEMM 4.2. code.

Magnetic saturation

The magnetic behavior of the materials is divided in two groups, non-magnetic and ferromagnetic. The first ones are not affected by the presence of a magnetic field, while the seconds are able to reoriented their magnetic dipoles enforcing the magnetic field created by an external excitation [13].
FEMM 4.2. code allows to treat ferromagnetic elements in two different ways, using linear relation or using real experimental curves of the magnetization of the material. The material used in the Hall Effect Thruster is the AISI 1010 and the magnetization curve is shown at 2.3.

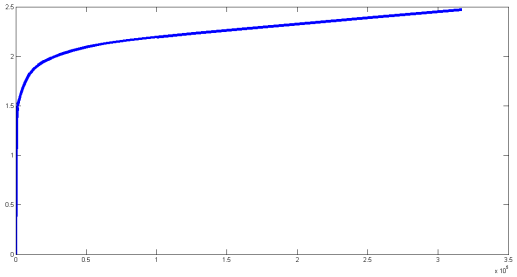

Figure 2.3: Magnetizacion curve AISI 1010.

where the I_0 stands for the current of the reference case and B_0 is the mean value of the magnetic field inside the chamber of the reference case
A bad design of the magnetic circuit could imply a non-linearity with the intensity because of losses of the magnetic field and consequently, power losses and magnetic deformations in the topology of the magnetic field (see Figure 2.4).
The optimum point is located along the linear relation of the actual line. This design will let all the magnetic circuit in saturation in the maximum regime of the operation of the thruster maximizing the weight of the magnetic circuit.

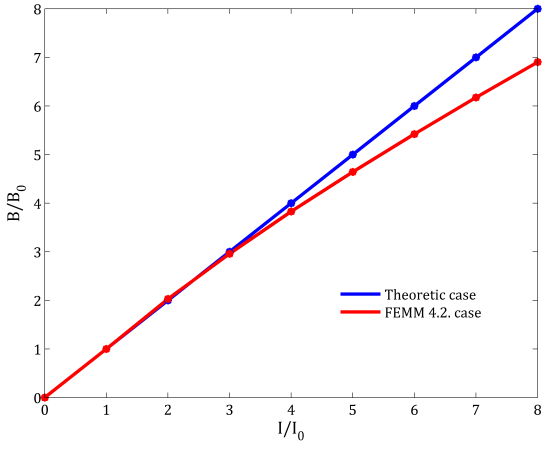

Figure 2.4: Evolution of the magnetic field as a function of the intensity.

Chapter 3

Studies of the Hall Effect Thruster

This chapter comprises the composition and location of the magnetic circuit of the thruster as well as some studies regarding those elements surrounding the chamber. In the case of the Hall Effect Thruster, no information of the position of each magnetic element was available. The baseline of the information used is just the actual shape of the chamber and the intensity and streamlines of the magnetic field. So, a trial and error process will be followed in order to get the desired specifications for the magnetic elements. Then, some studies related to the magnetic elements and magnetic topologies will be performed.
During this section the magnetic field intensity will be given in Tesla (T), because those units are the ones given in the images used by EP2 in previous studies.

3.1 Reference magnetic configuration

The only information available to reproduce the magnetic circuit of this thruster was related to the topology and the intensity of the magnetic lines inside the chamber and in the magnetic nozzle region. Images taken as reference are supplied by EP2 previous experiences and they are presented at Figure 3.1.
These images show the magnetic and the streamlines of the SPT 100, respectively.

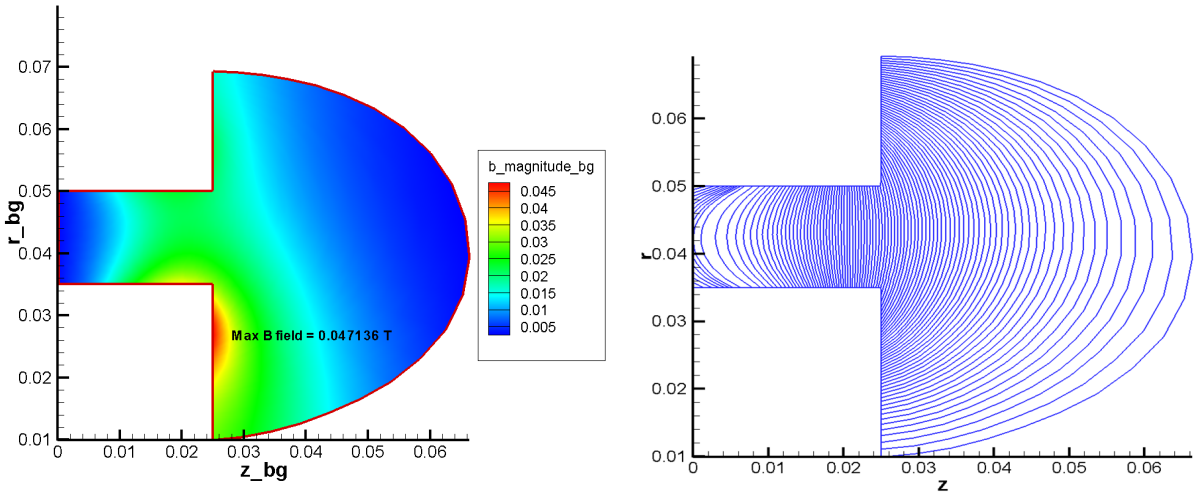

Figure 3.1: Magnetic field of a SPT 100 Thruster. Left figure: intensity of the magnetic field. Right figure: magnetic lines.

The main parameters extracted from the previous figures are the dimensions of the chamber (presented at Table 3.1).

OR	35 mm
IR	50 mm
L	25 mm

Table 3.1: Chamber dimensions of the SPT 100 Thruster.

where OR and IR are the outer and inner radius, respectively, and L is the length of the chamber.
Taking a look at the magnetic field characteristics, in the rear part of the thruster, there is a region in which the intensity (see equation 3.1) is approaching to zero. And, as expected, in the magnetic nozzle region, the value of the intensity of the magnetic field decreases as the distance to the chamber increases. In the exit of the chamber, the intensity of the magnetic field have the greatest value, this avoids the erosion with the walls of the chamber (see [16] for further information).

$$B(r,z) = \sqrt{B_r(r,z)^2 + B_z(r,z)^2} \tag{3.1}$$

where B(r,z) is the modulus of intensity of the magnetic field, $B_r(r,z)$ and $B_z(r,z)$ are the radial and the axial coordinate of the magnetic field, respectively.
Moreover, lines in the nozzle region go out from one of the solenoids and reach the other. At the same time, the line in the main part of the chamber are mainly pure radial, they change this behavior in the rear part of it. It is important to realize that all the figures presented in following sections have a different orientation with respect to the EP2 ones, the r-coordinates will be presented in the x-axis and the z-coordinates in the y-axis, while in Figure 3.1 are presented the other way around. This is related to the functioning of the FEMM 4.2. code as it establishes in the vertical axis.

3.2 Magnetic components of the Hall Effect Thruster

The Hall Effect Thruster is a 3D thruster. For simplicity, as it was explained previously at section 2.3.1, it is commonly analyzed as an axisymmetric problem. The scheme is as follow (Figure 3.2):

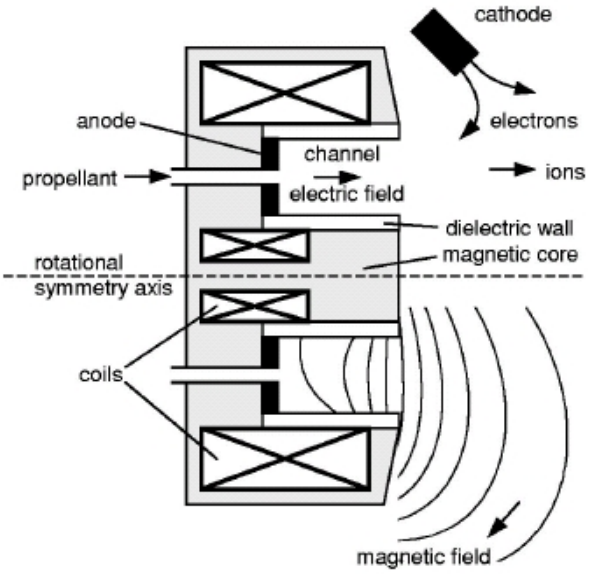

Figure 3.2: Scheme of a Hall Effect Thruster

In general, this type of thruster is composed by a magnetic core surrounding the complete chamber, different magnetic elements such as coils, solenoids, located in different positions depending on the kind of Hall Effect Thruster implemented, and a dielectric wall out of the scope of this analysis as it has no influence on the magnetic field. The different elements that can be found within the magnetic circuit and its function can be see at Table 3.2.

Element	Description	Advantage	Disadvantage
Solenoid	Long coil surrounding the thruster tube	Uniform inner magnetic field	Rapidly-divergent MN
Nozzle coil	Large-radius coil at the exit of the thruster tube	Allows control of magnetic throat and the MN divergence.	May deform the inner magnetic field.

Table 3.2: Basic magnetic generators. [22]

During this project, the HET that will be analyzed is the SPT 100 [12]. This thruster was developed in the USSR in 1982, and was capable of generate a thrust of around 83 mN. It only uses solenoids to generate the magnetic field because this allows to have the control of the intensity of the magnetic field. It is a thruster that has been simulated quite often with some important variations such as including magnetic shields or rear coils in order to vary the magnetic topology. This project will be based on these new additions.
The scheme of the magnetic circuit that will be used is presented at Figure 3.3..

- Magnetic coil.
- Solenoids located in different positions depending on the power required.

- Dielectric wall.
- Magnetic shield so as to modify the morphology of the magnetic lines.

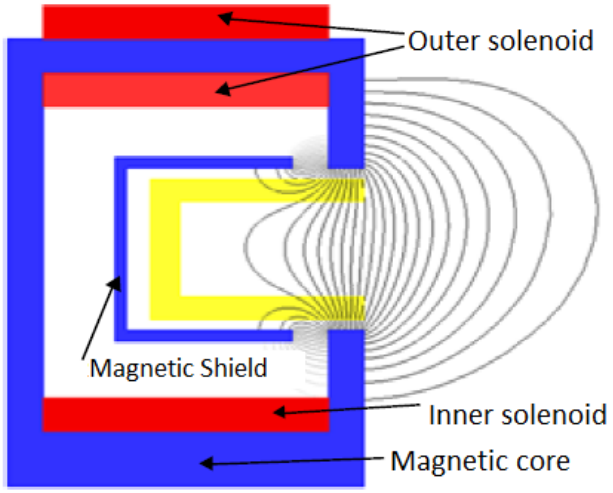

Figure 3.3: Scheme SPT 100 [21]

The revolution axis is located in the bottom part of the image.
Traditional HET (as SPT) developed to this moment have just an inner and an outer solenoid. In this thruster, an additional outer solenoid has been included. This new inclusion allows the increment of the efficiency of the thruster as it allows to have a greater control of the topology of the magnetic field than the traditional thrusters.
An additional internal solenoid could be included too, and it mainly affects the radial magnetic field inside the chamber (see [20] for further information). But, this addition will not be taken into consideration because of the thruster dealt with is a minithruster. This introduction will be complicated in a limited space and the emission of heat by Joule effect have not been studied yet.
Once the different elements used in the SPT 100 thruster are described, the location of those elements is going to be established. The information available at the beginning of this project is the dimensions of the complete thruster are the ones related to the chamber.
A first approximation of the dimensions and locations of the magnetic elements of the studied thruster can be obtained from Figure 3.3.
All the dimensions are presented in millimeters. The dashed line indicates the location of the chamber of the thruster and the dotted-dashed line indicates the axis of revolution.

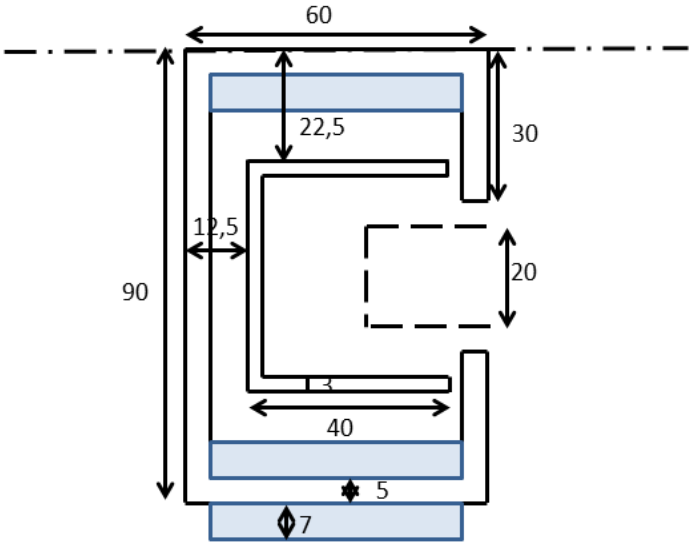

Figure 3.4: Dimensions for the Reference case

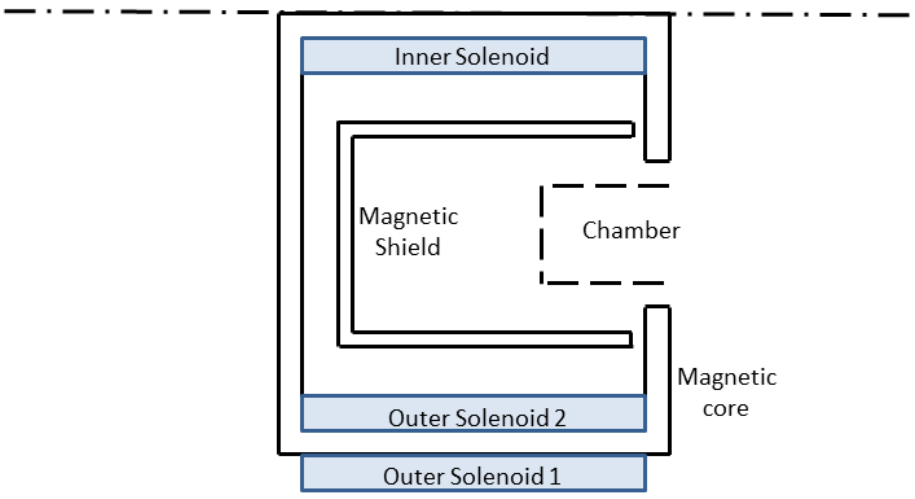

Figure 3.5: Names used hereinafter for the different magnetic elements of the SPT 100 thruster

In the following table the different wire parameters of the magnetic elements are presented:

Element	Cable parameters
Chamber	–
Outer Solenoid 1	AWG12 (d = 2.053 mm) $J = 972$ A · turns N = 108 turns
Outer Solenoid 2	AWG12 (d = 2.053 mm) $J = 972$ A · turns N = 108 turns
Magnetic shield	–
Inner Solenoid	AWG12 (d = 2.053 mm) $J = 3888$ A · turns N = 432 turns
Magnetic core	–

Table 3.3: Magnetic generators used with their characteristics and chamber location

$J = I \cdot N$, being N the number of turns and d is the diameter of the wire used.

No information about the cable wiring of chamber and magnetic field is given, since those element do not have wiring.

The material used to wire the solenoids and coils is copper (Cu) whose characteristics are high thermal and electrical conductivity, markedly higher than those of any other base metal and are exceeded only by silver. It is also a ductile material.

There is an important difference between the inner and the outer solenoids, and it is related to direction of the direction of the magnetic field. The inner solenoid the magnetic lines have a clockwise direction, while outer solenoids (1 and 2) are counterclockwise one. This is performed in order to emulate the nozzle streamlines of the images proportioned by EP2.

Magnetic core and magnetic shield are both made of AISI 1010 Steel. It is a low carbon steel that is mainly used in different pipelines, in construction after several treatments processes such as quenching, and in machine constructions.

The boundary conditions established far from the thruster are Dirichlet, meaning that far away the magnetic potential is set equal to zero.

The material used as environment is air, one of the predetermined materials of FEMM 4.2. The air has a relative linear magnetic permeability (in both r and z components) equal to 1 with the vacuum properties taken as the references ones. So, vacuum and air will imply no difference in the obtained results (see Figure 3.6).

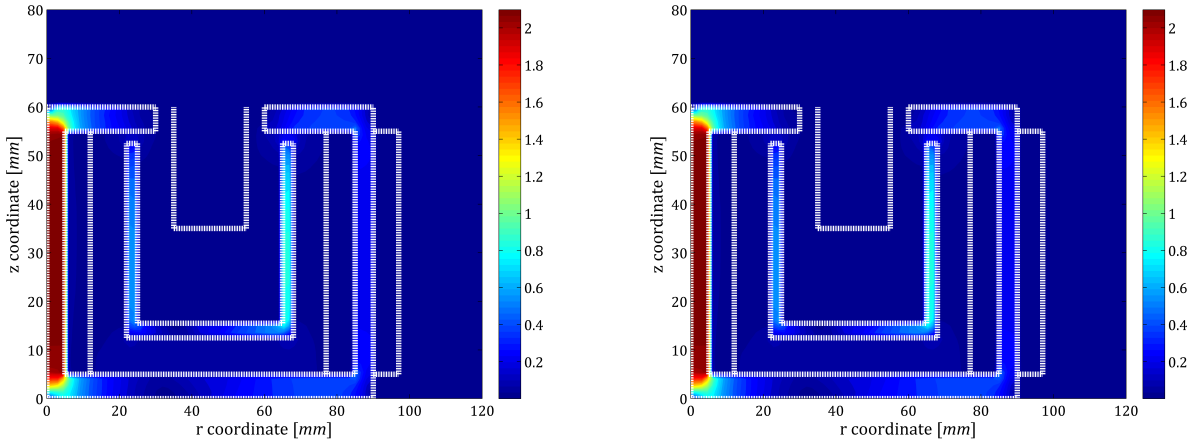

Figure 3.6: Comparison of the magnetic field using vacuum (left figure) and air (right figure).

The white lines represent the location and size of the different magnetic elements and the chamber of the thruster implemented. In all the figures showed during the present thesis, just half of the thruster is been represented due to the axisymmetry of the problem dealt with.
The results from the reference case are shown at Figure 3.7. Regarding the intensity of the magnetic field, the shape of it satisfies the desired one. In the rear part of the chamber, the values approaches to zero, while there is a peak 10 % lower than the expectations (see figure 3.1).

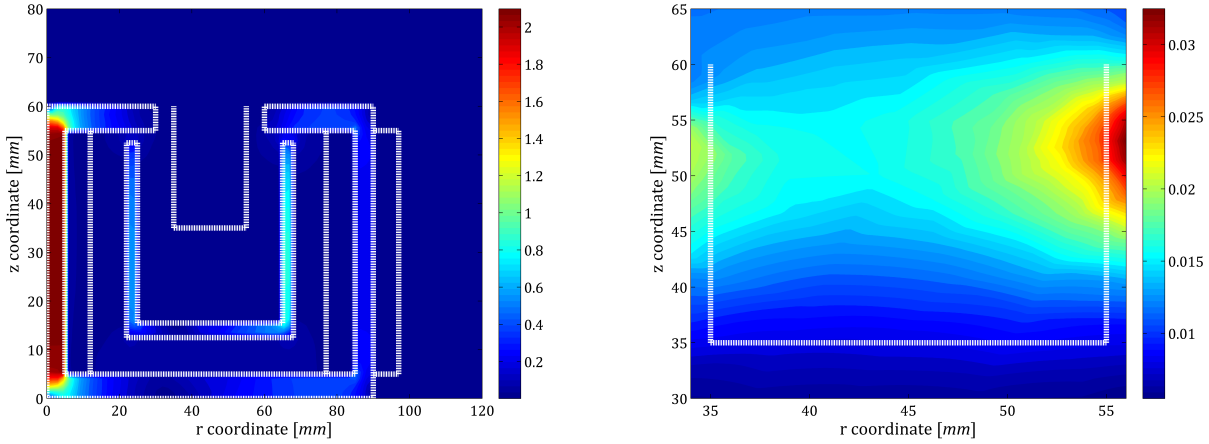

Figure 3.7: Magnetic field values of the reference case for the SPT-100. Right figure: zooming of the left one, focusing on the chamber region

In order to analyze the streamlines of the reference case (Figure 3.8), the chamber will be the only element represented and it is shown in black color. Been focused on the nozzle area, the streamlines are mainly axial. At the same time, the lines inside the chamber are also axial. This is not as desired, so several characteristics must be changed in order to get the expected streamlines.

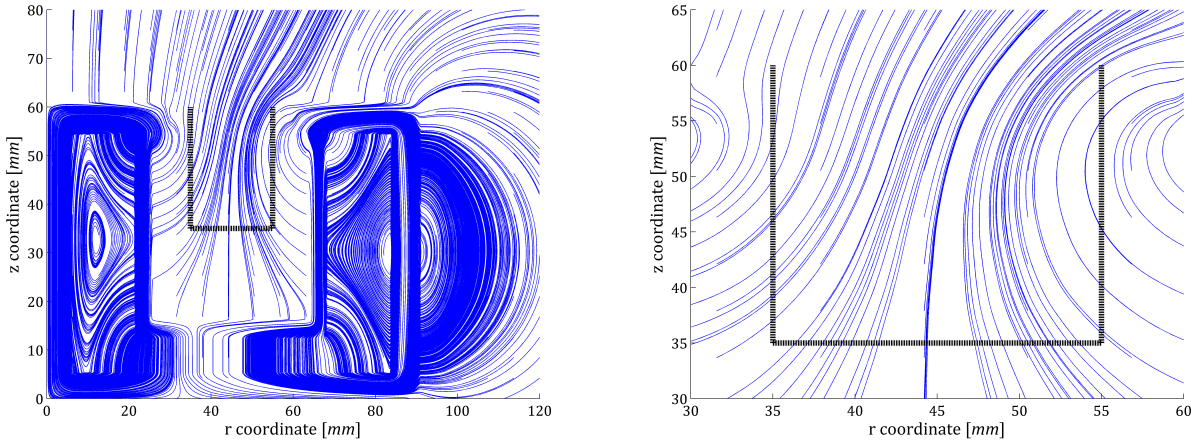

Figure 3.8: Streamlines of the reference case for the SPT-100. Right figure: zooming of the left one, focusing on the chamber region

3.3 Changes in the SPT 100 with respect to the reference case

As explained at section 3.2, there are some dissimilarities between the first trial model obtained in the previous section and the used by EP2 group in previous projects. So as to solve them, the trial and error method will be implemented. It is based on reaching a solution by trying out different possibilities until the error is small enough or even eliminated; or the agent stop working out.

The streamlines of the reference case should be changed in order to seem to the ones of EP2 images. Those lines must have a higher radial component instead of the axial one. For such a reason, the material of the magnetic shield is completely changed. The selected material is within the Neodymium magnet that is the most widely used in permanent magnets. In general, the Neodymium family are made from an alloy of neodymium, iron and boron. They are the strongest type of permanent magnet commercially available. Its main properties are high remanence (measure the strength of the magnetic field), higher coercivity (material's resistance to becoming demagnetized) but it has lower Curie temperature (the temperature at which the material loses its magnetism) than other commercialized types. The selected Neodymium among the different neodymium materials, the selected one is NdFeB32. The magnetization of the magnetic shield is axial pointing downwards, meaning that the magnetic lines of the permanent magnet go out from the lowest side of the magnet and they enter into the upper part.

Comparing the results from Figure 3.1, in the rear part of the chamber, the values of the EP2 are lower than the one of this case, this would be modified by changes in the magnetic shield. Moreover, in this case, there is a region where the intensity of the magnetic field reaches values of 0.09 T what implies that the peak is 45 % higher than the reference one (see Figure 3.1).

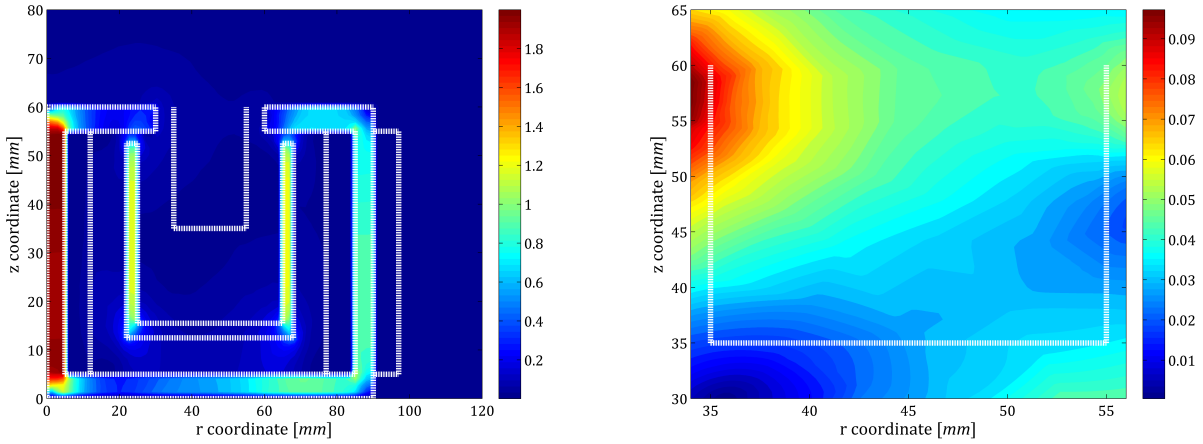

Figure 3.9: Magnetic field values with the material change of the magnetic shield. Right figure: zooming of the left one, focusing on the chamber region

In the nozzle area, the streamlines go out from one of the solenoids and reach the other, as it was expected from EP2 images. In the rear part, the lines are also pure axial while in the EP2 images they a have a lower radius of curvature. Moreover, there are two singular points close to the chamber, this will be corrected in further analysis.

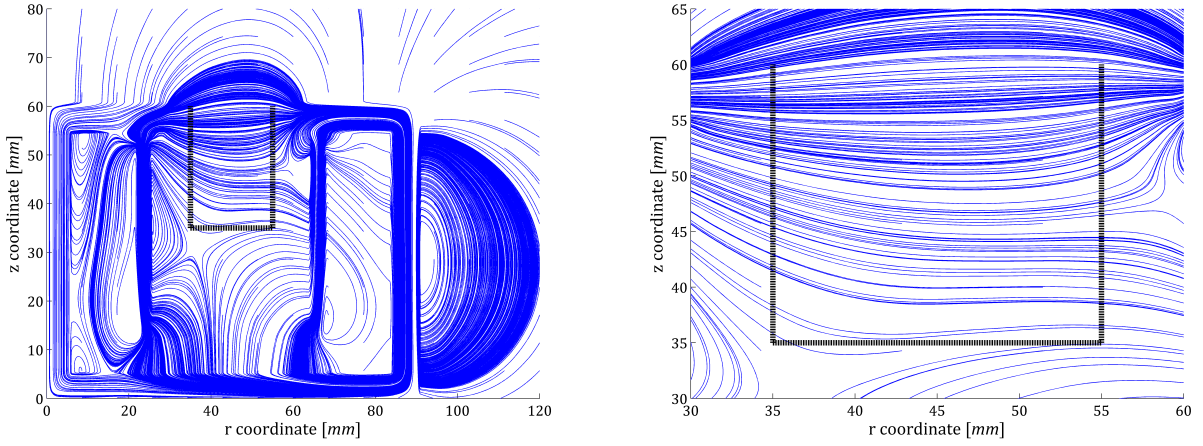

Figure 3.10: Magnetic field values with the material change of the magnetic shield. Right figure: zooming of the left one, focusing on the chamber region

For all these reasons, this change will be considered valid. And this case will be considered as the starting point from which all all the future modifications will be performed.
One of the main problems of the previous case is related to the location of the singular point in the right of the chamber. For this reason, the right arm of the magnetic shield is going to be reduce in size. Its size will be decreased in 20 mm. The results are shown at Figures 3.11 and 3.12.
Concerning the intensity of the magnetic field, the main difference with respect to the reference case is presented in the rear part of the chamber; this behavior is more similar to the one of interest (EP2 model) as there is a

complete area located in the rear part in which the value of B close to zero. Opposite to that new phenomena, there is no relevant difference related to the peak situated in the left side of the chamber.

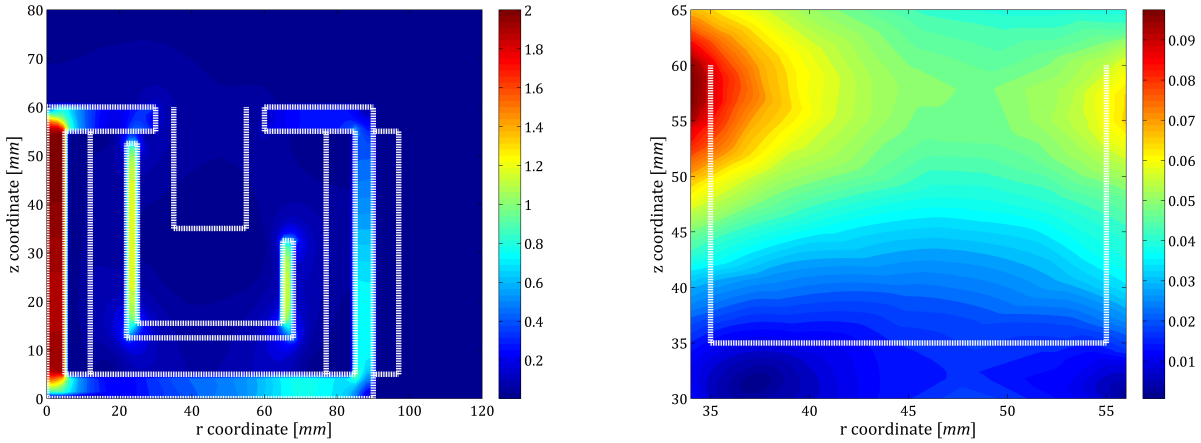

Figure 3.11: Magnetic field values of the decreased in size of the right arm of the magnetic shield. Right figure: zooming of the left one, focusing on the chamber region

In the case of the streamlines, as it was expected when the change was performed, the upper singular point has changed its position and now, it is located in the rear part of the chamber. On the other hand, the left hand-side singular point has now inside the chamber regime.

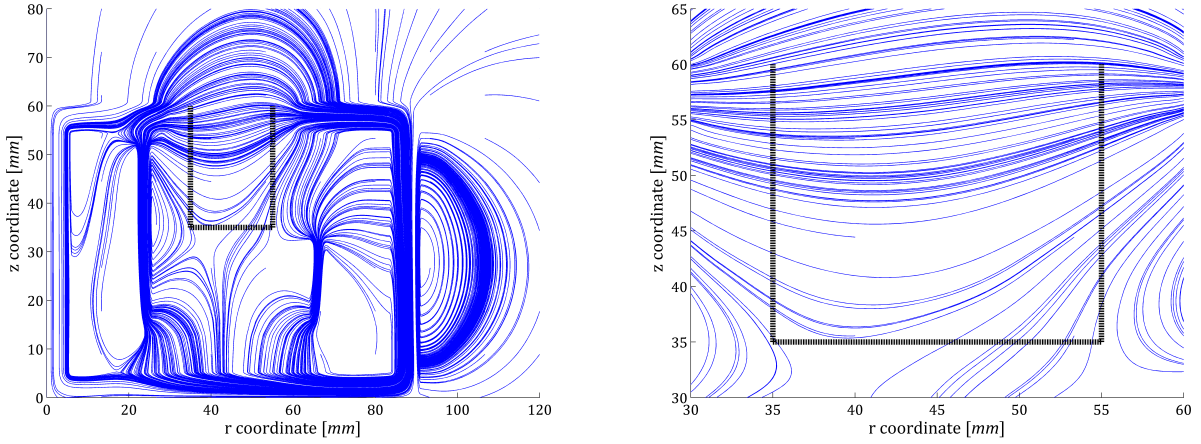

Figure 3.12: Streamlines of the of the decreased in size of the right arm of the magnetic shield. Right figure: zooming of the left one, focusing on the chamber region

Summarizing, this change will be kept as it is closer to the EP2 model.
The following modification is related to the left arm of the magnetic shield, as it was performed previously, this side is reduced 20 mm, so as to have again a symmetric magnetic shield. The results obtained are presented at Figures 3.13 and 3.14.
This change in the left arm produces significant modifications in both, the intensity of the magnetic field and

in the flux lines.
In the first case, the values of B in the rear part increases up to 0.03 in some cases. This is not a valid change as it differs from the EP2 images.

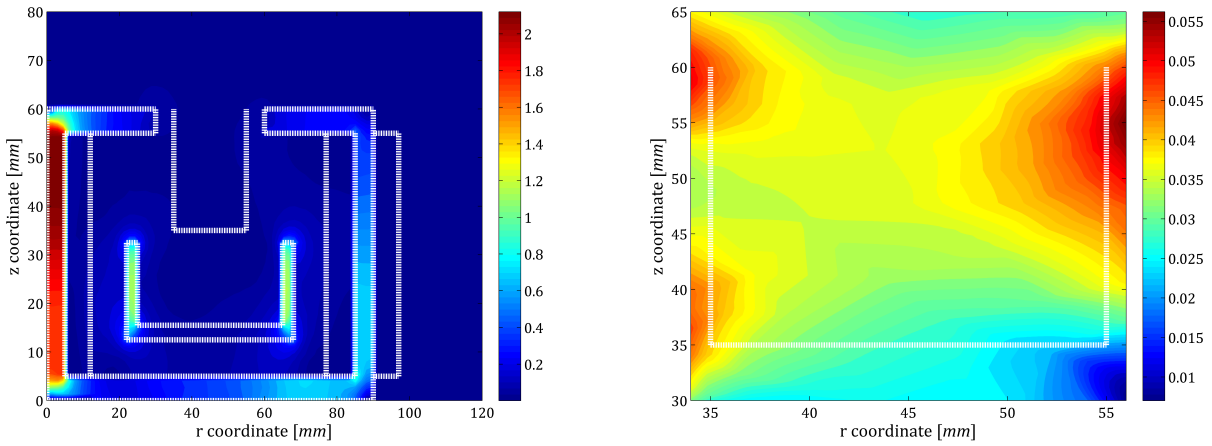

Figure 3.13: Magnetic field values of the decreased in size of the left arm of the magnetic shield. Right figure: zooming of the left one, focusing on the chamber region

Besides the singular points are further away from the chamber than in the previous cases, the streamlines inside the chamber are no longer radial and they have an inclination.

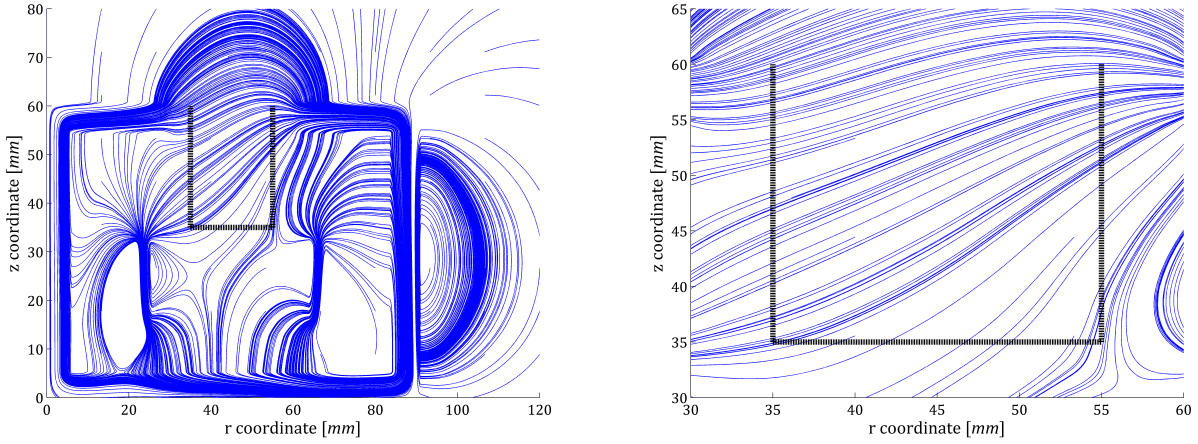

Figure 3.14: Streamlines of the of the decreased in size of the left arm of the magnetic shield. Right figure: zooming of the left one, focusing on the chamber region

Because of those reasons, this change will not longer be valid, so the following step will be performed with respect the non symmetric magnetic shield shown before.
The next modification is related to length of all the magnetic elements. The chamber of the thruster is not included in that change and it will keep constant in size and position (r and z component), meaning that an increase in the length of the elements will imply that they are located in negative z-coordinates, as it is the

following studied case. During this modification, the length will increase 20 mm too.
The intensity of the magnetic field follows the same behaviour as in the second studied case (in which the right arm of the magnetic shield was increased), its value is close to zero in the rear part of the chamber and there is a peak in the left side, close to the exit. Besides that peak of intensity, the shape of it seems to the EP2 intensity.

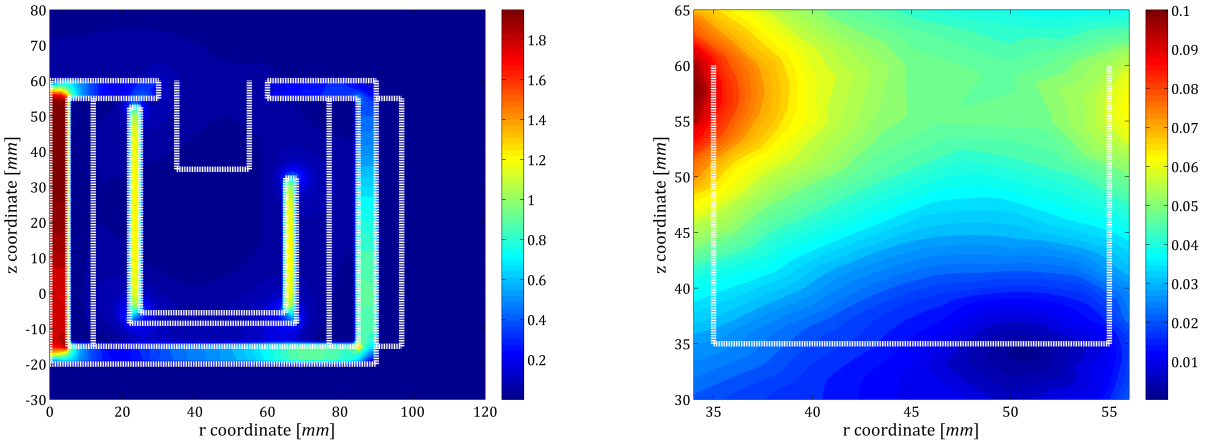

Figure 3.15: Magnetic field values of the increase in length of all the magnetic elements of the SPT 100. Right figure: zooming of the left one, focusing on the chamber region

Although the shape of the intensity fits well with the goal, there is a singular point close to the rear part of the thruster, which must be eliminated in further studied cases, while the other is further from the chamber, for this reason, this change will be retained for the next studies.

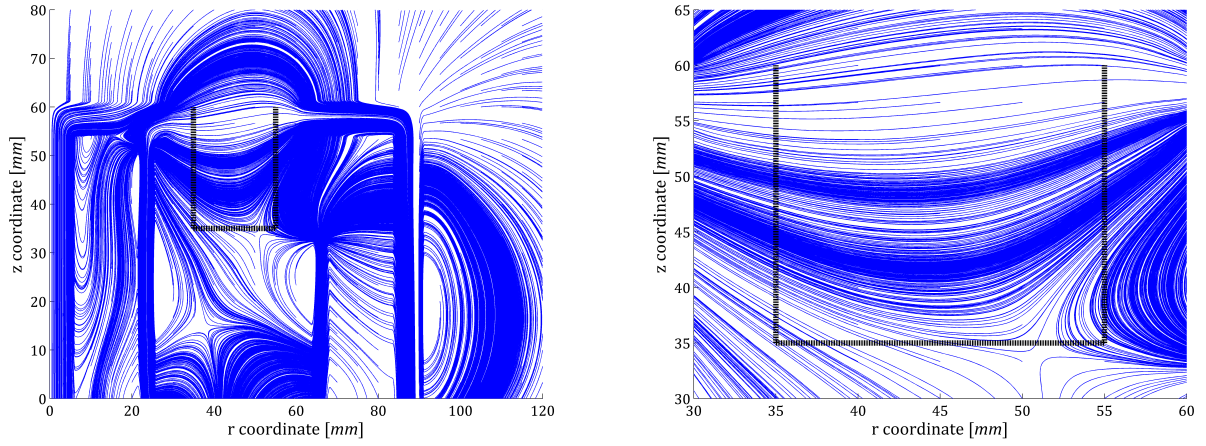

Figure 3.16: Streamlines of the of the increase in length of all the magnetic elements of the SPT 100. Right figure: zooming of the left one, focusing on the chamber region

As it was explained earlier, changing the left arm of the magnetic shield is not an appropriate solution so as to move the singular point. Consequently, a more convenient way could be increasing the OR of all the

magnetic elements involved in the analysis. This implies that the r-coordinates of the chamber will be changed in order to maintain the symmetry (concerning the location) with respect to r-coordinate. So, the change is an increased in OR of 10 mmm, and, consequently, a change in the chamber of 5 mm in both the inner and the outer radius.

The intensity of the magnetic field is presented at Figure 3.17. In the left side rear part of the chamber, there are points with a values which doubles the expected one, and on the other hand in the right part those values are as supposed, this means that this change present less accurate results in terms of intensity that the previous one, for such a reason this change is rejected.

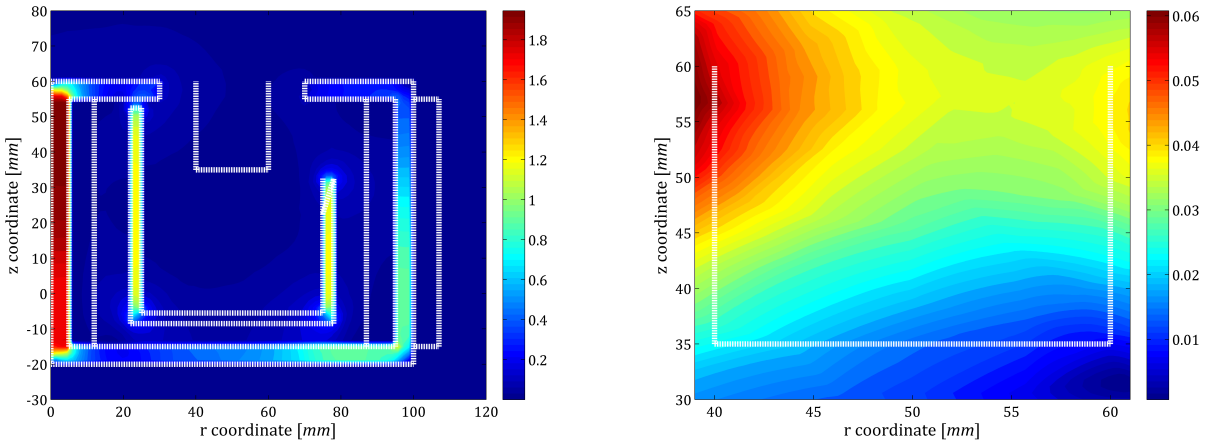

Figure 3.17: Magnetic field values of the increase in the outer radius of all the magnetic elements of the SPT 100. Right figure: zooming of the left one, focusing on the chamber region

Opposite to the intensity analysis, the right hand-side singular point gets away from the chamber of the thruster, as it was desired. On the other hand, the lines going from one solenoid to the other acquiring more ellipse shape which do not satisfy the EP2 images.

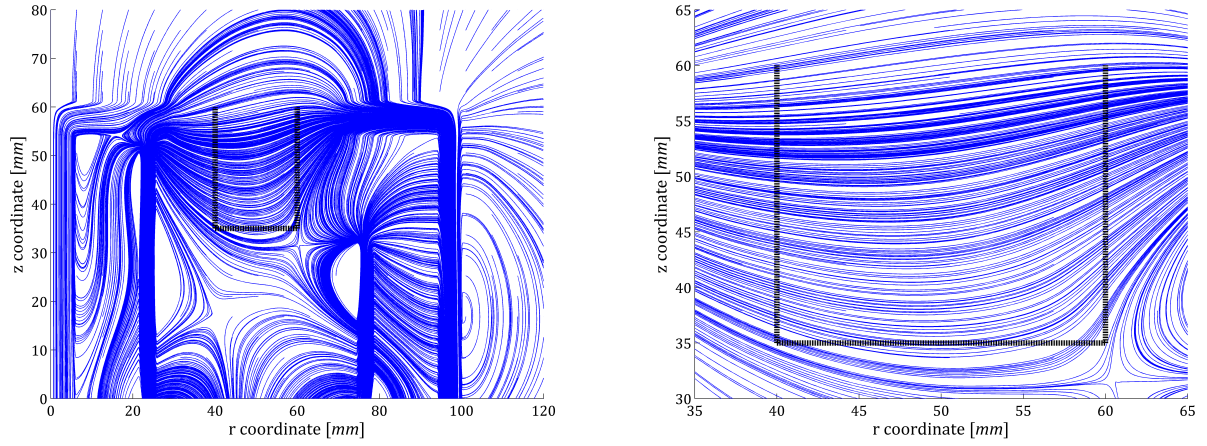

Figure 3.18: Streamlines of the of the increase in the outer radius of all the magnetic elements of the SPT 100. Right figure: zooming of the left one, focusing on the chamber region

For all those reasons, these change will not be kept.
Up to this point, one of the singular point is located close to the rear part of the chamber of the thruster; this problem should be avoided if possible. So as to do so, the right hand side of the magnetic shield is going to be reduced again. This side is reduce in 10 mm.
Regarding the intensity of the magnetic field, the only difference with respect to the expected one is related to the peak close to the exit of the thruster that will be try to solve in later analysis, because it reaches a value of 0.098 T, a 48 % higher than the expected one (compared to the EP2 model).

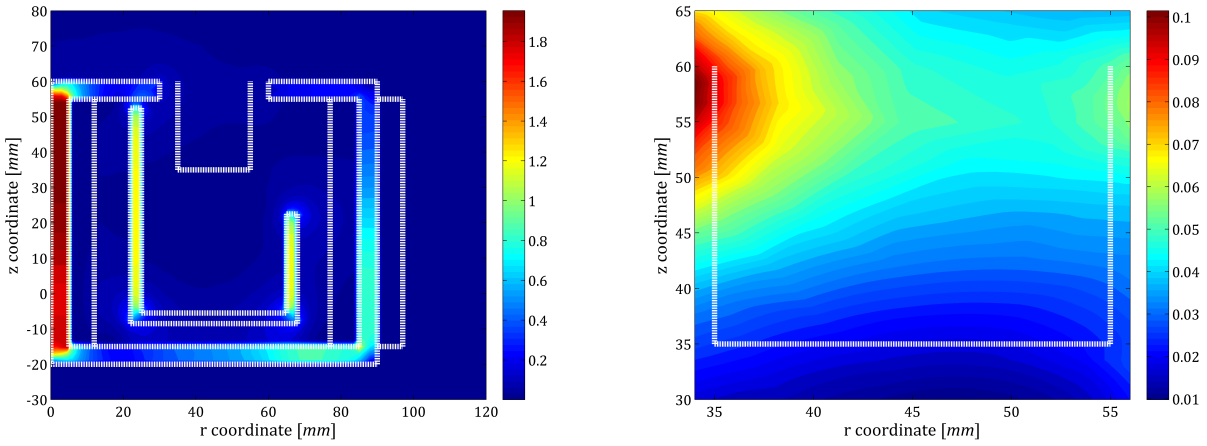

Figure 3.19: Magnetic field values of the decrease in length of the right arm of the magnetic shield. Right figure: zooming of the left one, focusing on the chamber region

With this change, singular points are kept far away from the chamber of the thruster. Moreover, the lines close to the exit are mainly radial and in the rear part have a radius of curvature that is increasing as the z-coordinate increases (as the EP2 model).

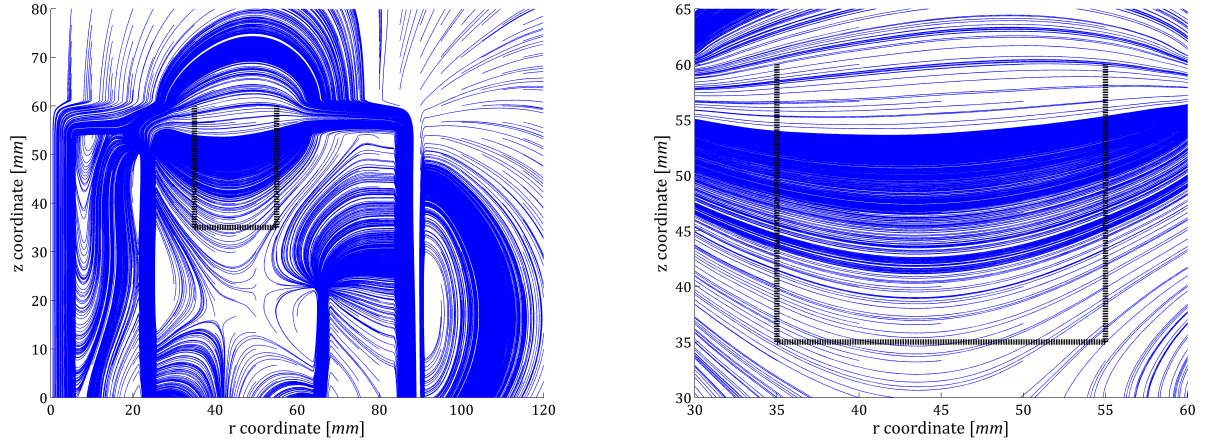

Figure 3.20: Streamlines of the of the decrease in length of the right arm of the magnetic shield. Right figure: zooming of the left one, focusing on the chamber region

In all the previous cases, there is a peak in the left hand-side exit of the chamber. In order to avoid it, the reduction in size of the left hand-side magnetic elements are going to reproduced. In order to do so the following changes have been performed, they are also represented at Figure 3.21

- the left arm of the magnetic shield is moved 10 mm to the left.
- the left arm of the magnetic core (upper part is not included) is kept in the same position but the h (dimension of the material) is reduced in 2 mm, meaning that the final length is 3 mm.
- the inner solenoid is also reduced in size. It is decreased in 4 mm, which implies that the final length is, also, 3 mm.

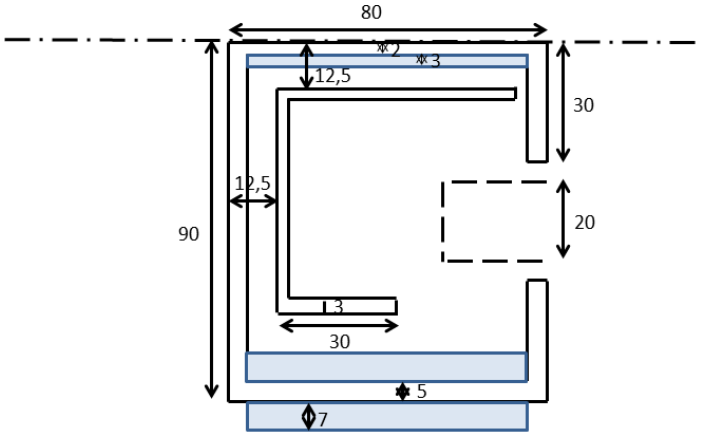

Figure 3.21: Scheme of a change referred to the inner part of the SPT 100 thruster. Right figure: zooming of the left one, focusing on the chamber region

The results obtained are presented at Figure 3.22 and Figure 3.23.
The main goal of this change was related to eliminate or reduce the peak in the upper part of the right hand-side image. In this case, the maximum value inside the chamber is 0.0448 T, meaning that there is 51 % with respect to the previous analysis. On the same way, the right hand-side rear part of the chamber is also reduced which is not an appropriate behavior because of wall-particles collisions in that area, which have an adverse effect on the thrusters life.

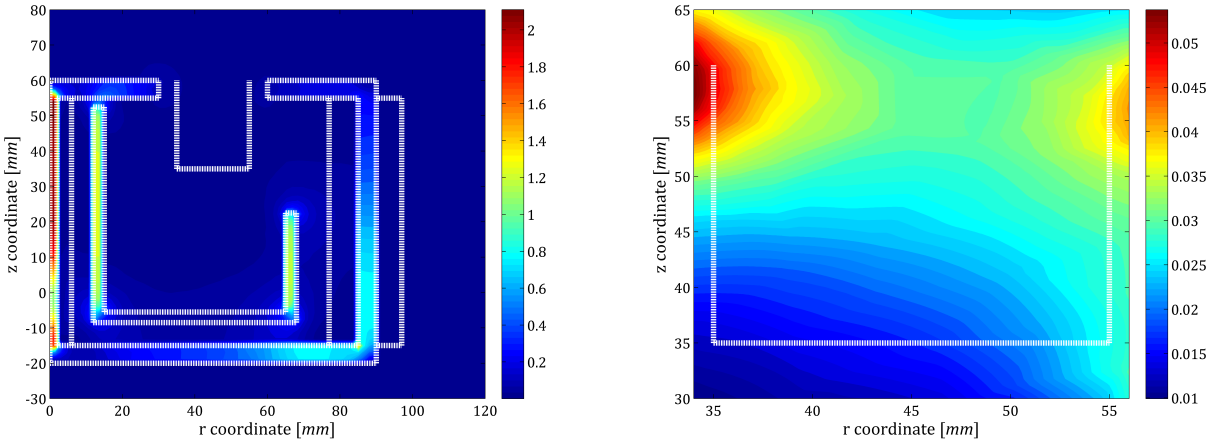

Figure 3.22: Magnetic field values of the decrease in size of all the magnetic elements located in the left hand-side. Right figure: zooming of the left one, focusing on the chamber region

Moreover, streamlines inside the chamber are no longer radial and the have a radius of curvature all along the chamber. For those reasons, this changes will be discarded.

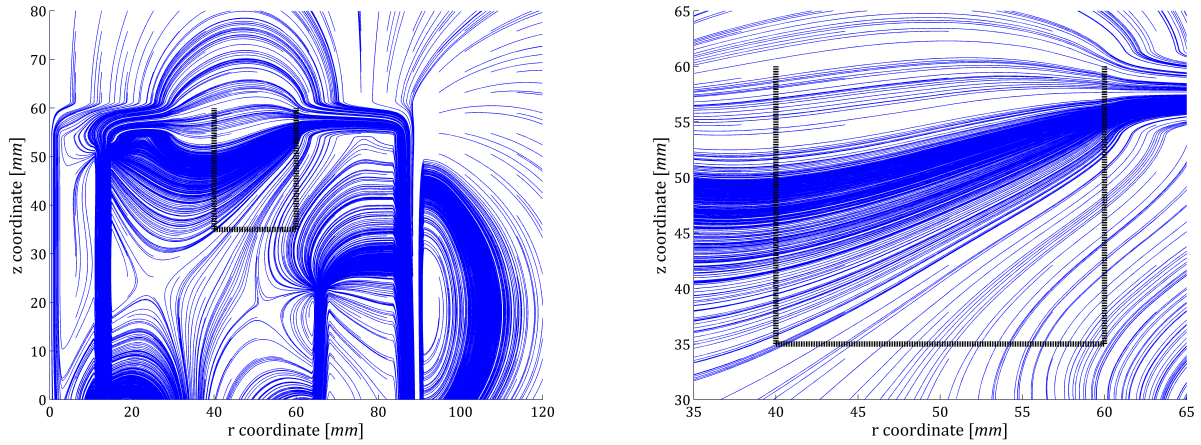

Figure 3.23: Streamlines of the of the decrease in size of all the magnetic elements located in the left hand-side. Right figure: zooming of the left one, focusing on the chamber region

Another way to avoid having the peak could be changing the magnetic properties of the inner solenoid. As it will be explained at 4.2.3, the most relevant parameter in solenoid is J, and this change will provoke a change in the magnetic field. For that reason, the intensity of the inner solenoid will be constant while the number of turns will be changed to 250 turns in a clockwise direction.
Once again, when this change is applied, there is a reduction of -33 % in the peak (the maximum value inside the chamber is 0.0665 T). In addition to that, the behavior of the magnetic field is kept constant and similar to the desire one (EP2 model). Consequently, from the point of view of the intensity and shape of the intensity of the magnetic field, this distribution of magnetic elements is considered valid.

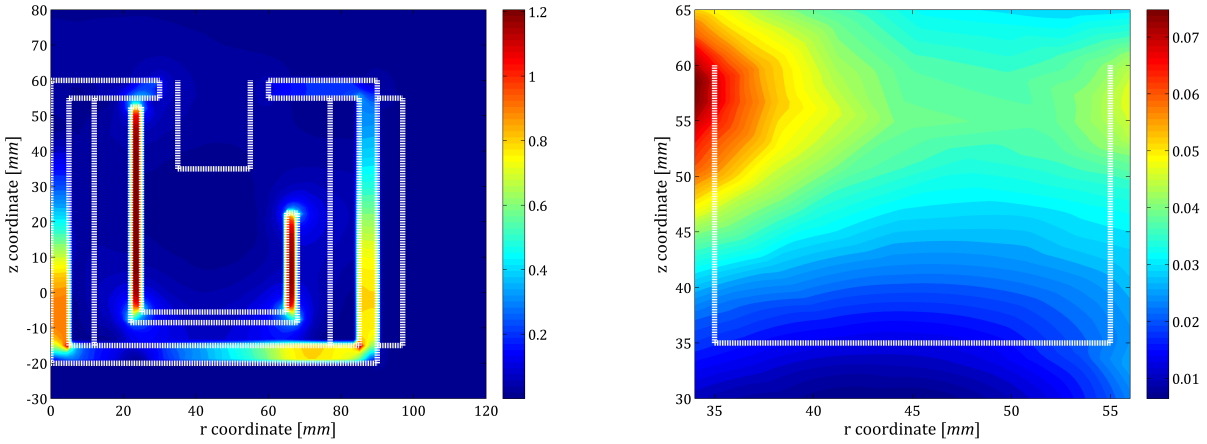

Figure 3.24: Magnetic field values of the decrease in size of all the magnetic elements located in the left hand-side. Right figure: zooming of the left one, focusing on the chamber region

Regarding the streamlines, both singular points are located far from the rear part of the chamber. Inside the chamber, the streamlines are mainly radial close to the exit of the thruster (z = 45 mm), below this value they have a radius of curvature. Opposite to the behavior of EP2 streamlines, these ones are no symmetric this is related to the non-symmetry at $r = 45mm$ of the analysis problem because of the shape of the magnetic shielding.

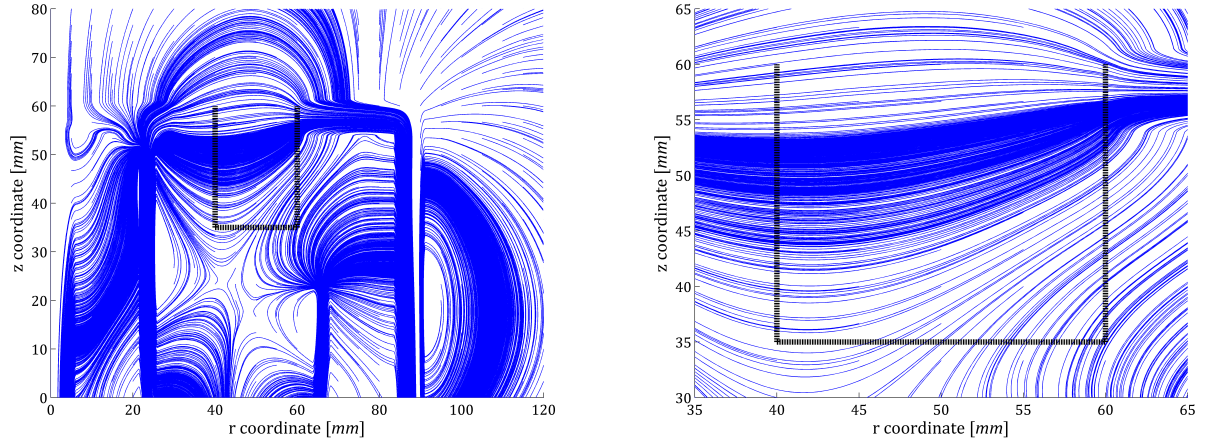

Figure 3.25: Streamlines of the of the decrease in size of all the magnetic elements located in the left hand-side. Right figure: zooming of the left one, focusing on the chamber region

The limit of the number of turns of this example (N = 250 turns) and it is mainly related to the streamlines. The lower the number of turns of the inner solenoid while the outer solenoids are kept constant, implies that the streamlines close to the exit have a lower radius of curvature, meaning that they are no longer radial (Figure 3.26). So, for that reason, there is a trade of study between the radial behavior of the streamlines and the reduction of intensity of the peak.
On the same way, a change in the number of turns in the inner and outer solenoids implies a change in the

shape and intensity of the magnetic field (Figure 3.27).

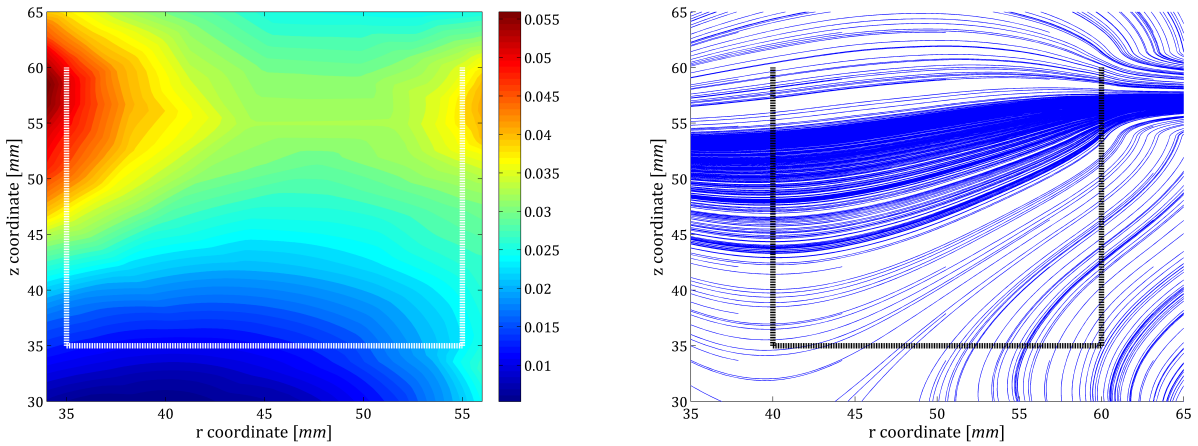

Figure 3.26: Magnetic field values and streamlines inside the chamber of the change of the number of turns in the inner N = 150 turns (clockwise). Right figure: zooming of the left one, focusing on the chamber region

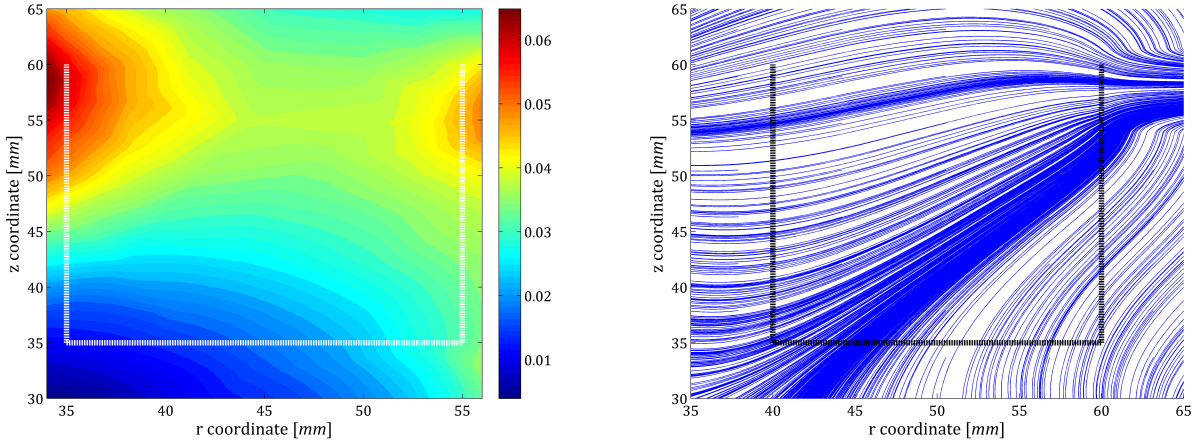

Figure 3.27: Magnetic field values and streamlines inside the chamber of the change of the number of turns in both the inner and outer solenoids. Inner solenoid: $N = 150 turns$ (clockwise) and outer solenoid: $N = 50 turns$ (counterclockwise). Right figure: zooming of the left one, focusing on the chamber region

For all that, the inner solenoid has a number of turns of 250 and the outer ones are kept with the same number as previously studied.
After all this analysis, the dimensions of the closest to the desire SPT-100 images from EP2 are presented at Table 3.4.

Element	Wiring parameters
Chamber	–
Outer Solenoid 1	AWG12 (d = 2.053 mm) $J = 972$ A · turns $N = 108$
Outer Solenoid 2	AWG12 (d = 2.053 mm) $J = 972$ A · turns N = 108 turns
Magnetic shield	–
Inner Solenoid	AWG12 (d = 2.053 mm) $J = 2250$ A · turns N = 250 turns
Magnetic core	–

Table 3.4: Final characteristics of the magnetic generators used

And the final dimensions are presented at Figure 3.28

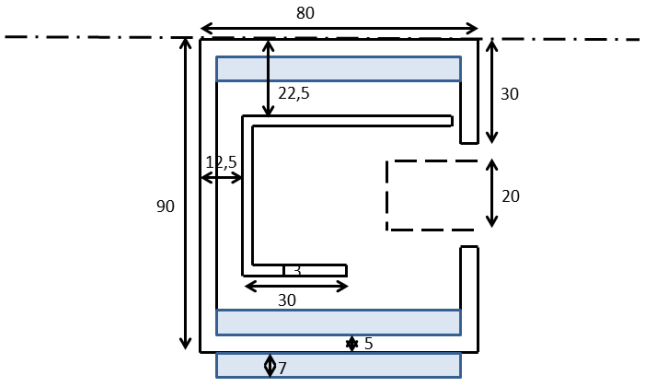

Figure 3.28: Final dimensions of the SPT 100 thruster.

Summarizing this section, all these changes developed before have as main objective look for a thruster as similar as possible to the EP2 used in previous studied.
At the end, focusing on just one half of the thruster (as it is presented in all the figures) the thruster obtained is not symmetric with respect to the mean line of the chamber ($r = 45$ mm), this foments the antisymmetry of the streamlines in the rear part of the chamber. Moreover, close to the exit of the thruster, the lines are mainly radial (as expected). And at the magnetic nozzle region, the lines have a radius of curvature that goes from one solenoid to the other, in this part the antisymmetry could be also appreciated.
In the case of the intensity of the magnetic field, there are also some similarities and some differences. The main clash is related to the peak located in the left hand-side exit of the chamber, this value is a 44 % higher than the one of EP2. Moreover, the values at the exit are 25 % higher than the desire ones. This values could not be reduced by neither geometry changes in the left hand-side magnetic elements nor properties changes of both inner and outer solenoids. Opposite to that, the rear part of the chamber looks similar to the desire one, values tend to zero as r decreases inside the chamber.

3.4 Analysis of the magnetic elements

Once the different parameters of the magnetic elements implemented in SPT-100 are been established at section 3.3, some studies will be considered.

3.4.1 Different studies related to magnetic core

The magnetic core studied previously is a solid structure made of AISI 1010 and forming a C-shape.
An study could be focused on the right and left ends of that shape. Up to this moment, they finished in a straight and horizontal line and it will be modified into an inclined line. This changed could be extracted from other images of the same SPT-100 model used by EP2 in previous analysis (Figure 3.29). In both figures, radial component and modulus of the magnetic field, there is a inclined line where the magnetic core is located.

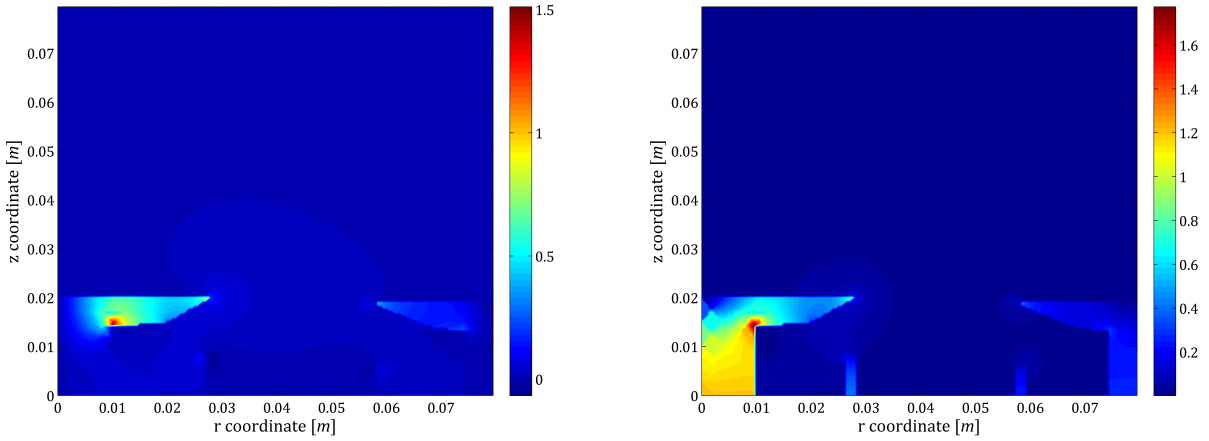

Figure 3.29: Magnetic field of a SPT-100 given by EP2. Left: r-coordinate of the magnetic field. Right: Intensity of the magnetic field.

In order to follow this change, this parameter will be set as:

$$\alpha = \arctan(\frac{5}{10}) = 26.56^{\circ} \tag{3.2}$$

where α is the angle forming the inclined angle with the horizontal line.
The adjacent leg is equal to 10 mm and the opposite one is equal 5 mm (the solid part of the magnetic core).

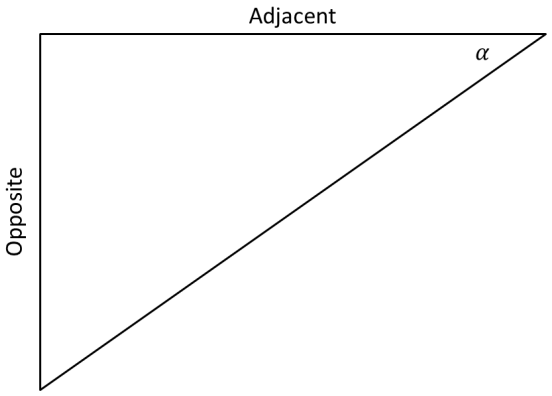

Figure 3.30: Triangle model for the inclined side of the magnetic core.

When this change is applied, the behavior of the modulus of the magnetic field do not experience any changes. In the rear part, those values tend to zero as the z-coordinate decreases; and moreover, there is a peak close to the exit of the chamber. But, there is a difference with respect the value of the peak, when this change is applied, there is a decrease of 15 % of that value with respect to the previous case.

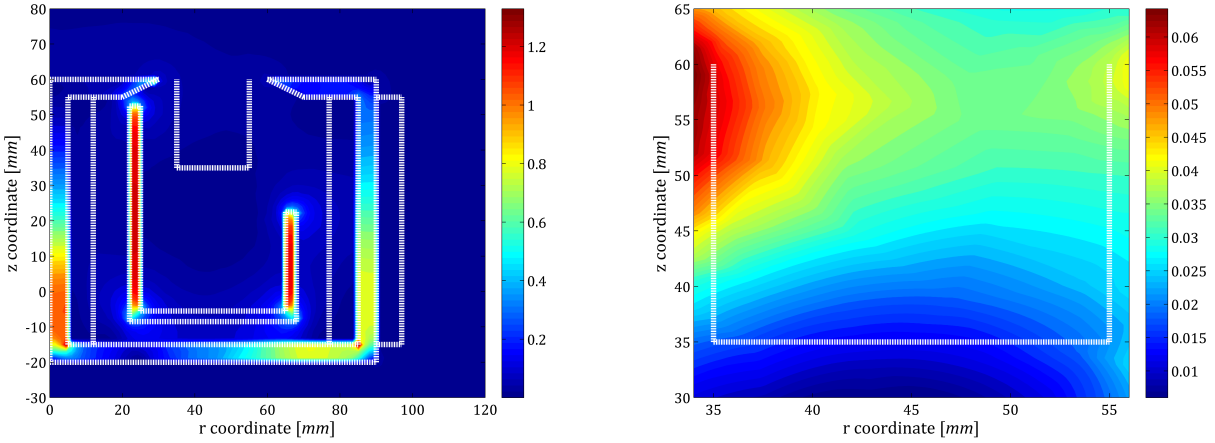

Figure 3.31: Magnetic field values of the change of the end of the C-shape of the magnetic core. Right figure: zooming of the left one, focusing on the chamber region.

In the streamlines, there is a significant change when this modification is been realized. It is related whith the streamlines inside the chamber. In the new reference case (the conclusion model from the previous section), streamlines were not symmetric with respect to $r = 45$ mm, they were displaced towards the left. Contrary to that, in this study lines are less displaced towards the left and its symmetry is closer to the corresponding r-coordinate. This adds more similarities with respect to the EP2 model, as expected from Figures 3.29. At the same time, streamlines located in the nozzle area are also symmetric with respect to $r = 45$ mm as the z coordinate increases.

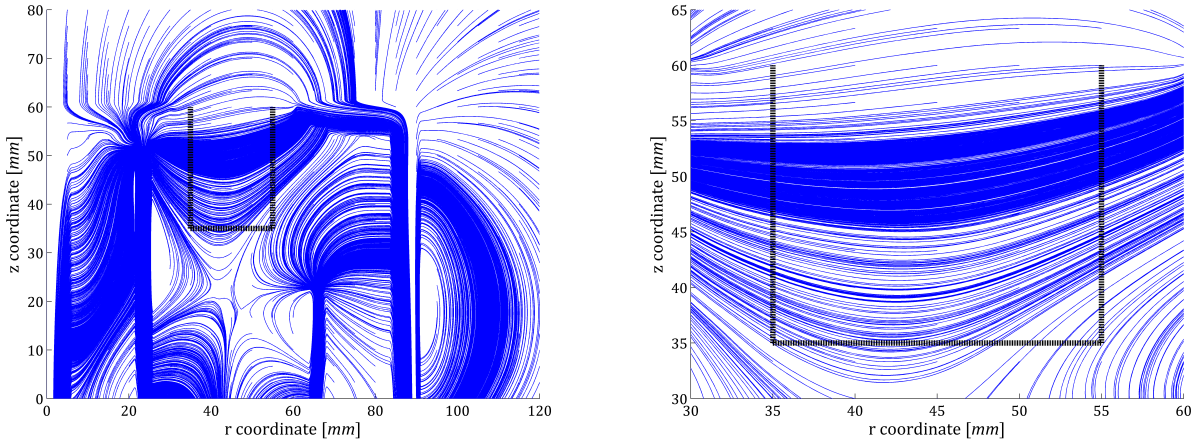

Figure 3.32: Streamlines of the change of the end of the C-shape of the magnetic core. Right figure: zooming of the left one, focusing on the chamber region.

Besides, the images proportioned by the EP2 group have a particular configuration for the end side of the magnetic core, some others will be analyzed, such as, non-symmetric configuration or changing the slope of the inclined end. In all the cases, the angle α is kept constant in the selected value.
The results of the change in the slope do not differ to much with respect to the previous inclined end (Figure 3.33). The different could be appreciated regarding the streamlines (Figure 3.34). When the slope is changed in sign, streamlines located z = [45-55] mm have a higher radius of curvature, and even, they passes from concave to convex as the z coordinate is increased.

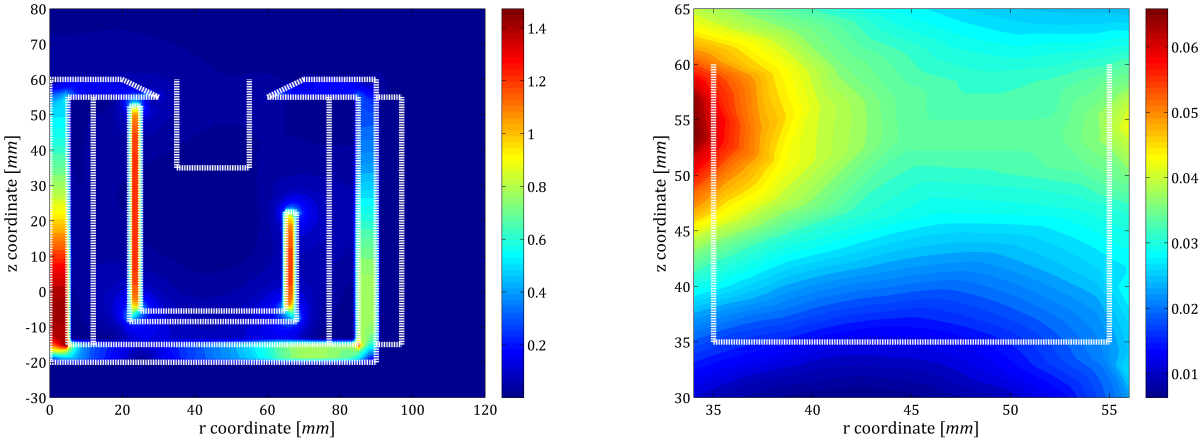

Figure 3.33: Magnetic field values of the change of the end of the C-shape of the magnetic core. Right figure: zooming of the left one, focusing on the chamber region.

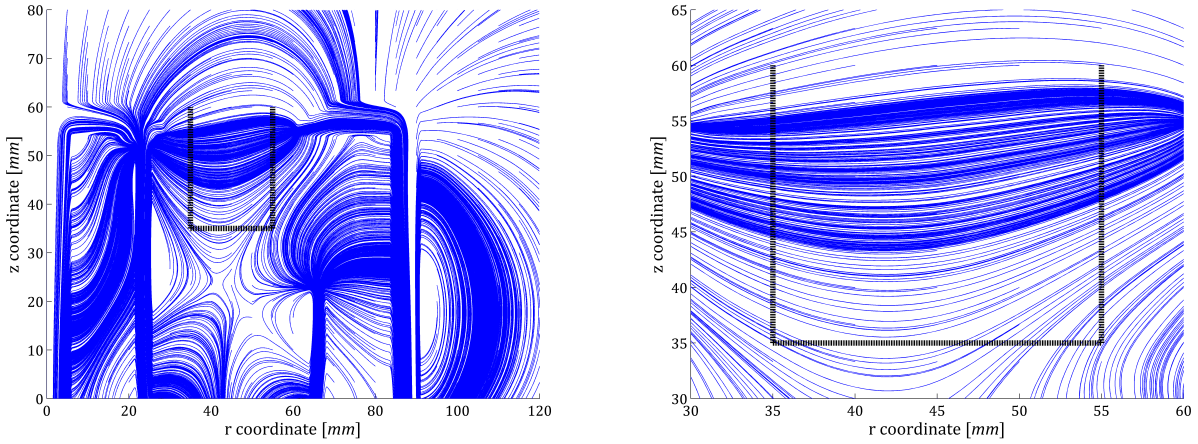

Figure 3.34: Streamlines of the change in the slope of the end of the magnetic core. Right figure: zooming of the left one, focusing on the chamber region.

Now, the antisymmetric problem will be analyzed. The end side with the inclined side is as the first example, while the other side has a infinitive slope.
The results of the intensity of the magnetic field are just presented inside the chamber because it is the area of interest (see Figure 3.35). Outside of it, the magnetic field remains with no changes. In the problem where the right is inclined, the only difference with respect to the having both ends inclined is related to the peak located in the right side of the chamber. This peak increases its value in a 17 %. On the other hand, when the inclined end side is placed in the left one, differences are placed in the rear part. The values of the magnetic field in the right part of the chamber decreases with respect to the reference one.
Although the change are exactly equal in both end sides, the behavior of the magnetic field is not the same because of the non-symmetry of the magnetic core.

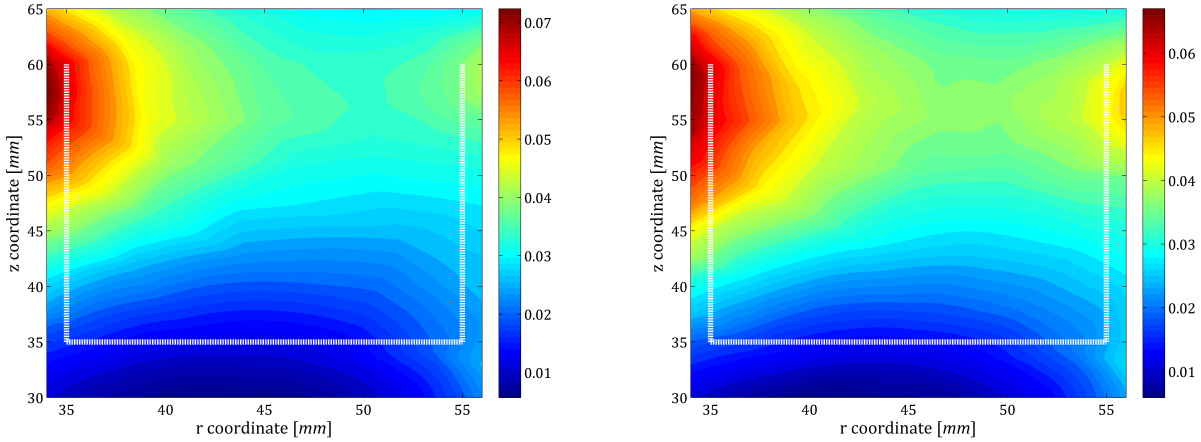

Figure 3.35: Magnetic field values of the change of one of the ends of the magnetic core. Right figure: inclined side located in the right side. Left figure: inclined side placed at the left side.

Analyzing the streamlines, just the inside chamber is represented too because of the same reason explained

previously. At the same time, there is no significant difference inside the chamber.

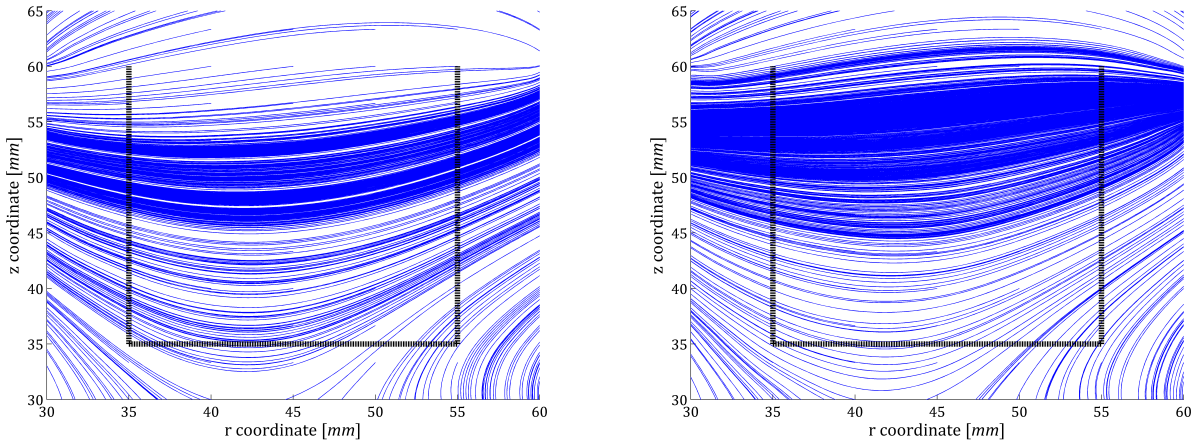

Figure 3.36: Streamlines of the change of one of the ends of the magnetic core. Right figure: inclined side located in the right side. Left figure: inclined side placed at the left side.

Secondly, an investigation related to the rear part of the thruster, this means, the rear part of the magnetic shield and the magnetic circuit will be analyzed. Regarding this elements, a first consideration eliminating just the rear part of the magnetic shield is going to be analyzed. So, in this case, the analyzed case will be presented at Figure 3.37.

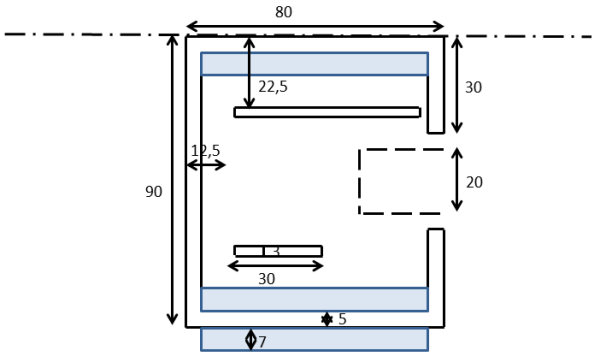

Figure 3.37: Scheme of the analyzed problem. The rear part of the magentic shield is been deleted.

When one of the magnetic element change its form, the magnetic field topology significantly changes. This is the case of the performed study. Regarding the intensity of the magnetic field, the peak in the left hand side part of the chamber increases its value in 65 %. The rear part is no longer uniform and and it does not tends to zero, because in the left hand-side, the intensity reaches values of 0.045 T.

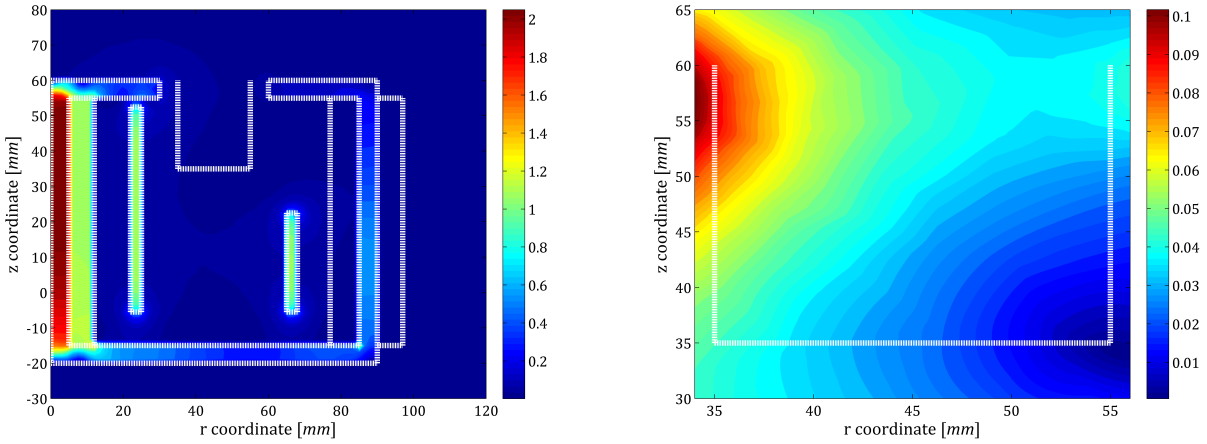

Figure 3.38: Magnetic field values suppressing the rear part of the magnetic shield. Right figure: zooming of the left one, focusing on the chamber region.

It happens the same with the streamlines. The singular point, located previously far from the chamber, in this case it enters into it. Moreover, streamlines in the rear part changes its orientation while in the central region of the chamber they move towards the right.

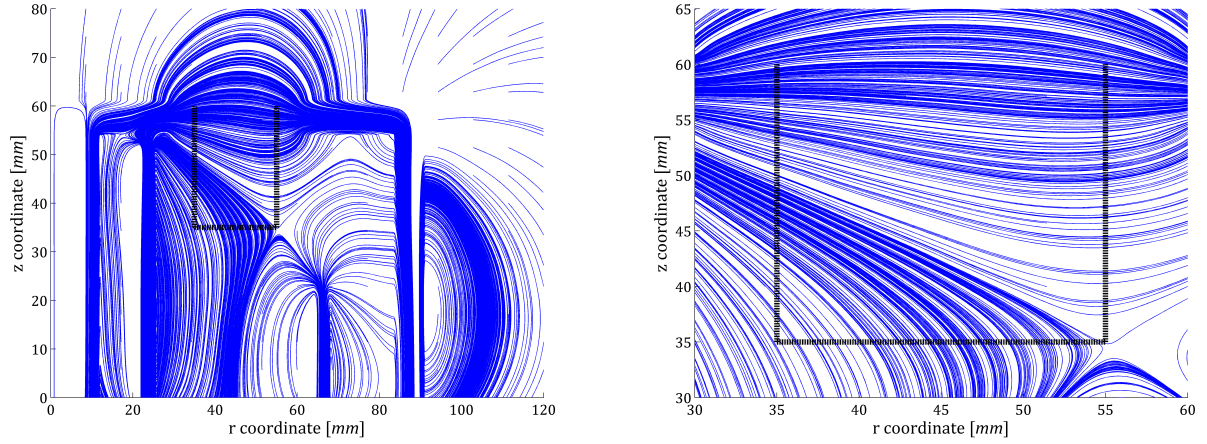

Figure 3.39: Streamlines suppressing the rear part of the magnetic shield. Right figure: zooming of the left one, focusing on the chamber region.

In this research, both, the magnetic core and magnetic shield will have no rear part.
In the case of the intensity of the magnetic field, the change is even more dramatically than in the previous study. The complete right side of the chamber acquires values close to zero. However, the peak keeps the same value as previosly mentioned.

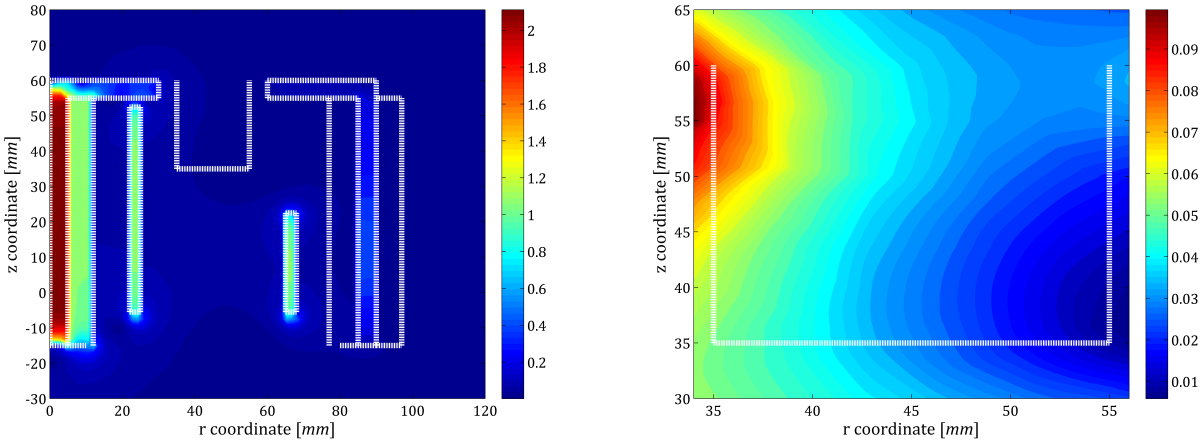

Figure 3.40: Magnetic field values suppressing the rear part of the magnetic shield and magnetic core. Right figure: zooming of the left one, focusing on the chamber region.

The streamlines of it follow the same behavior of just removing the rear part of the magnetic shield. In the central region, streamlines move towards the right and in the rear part, they have a lower radius of curvature.

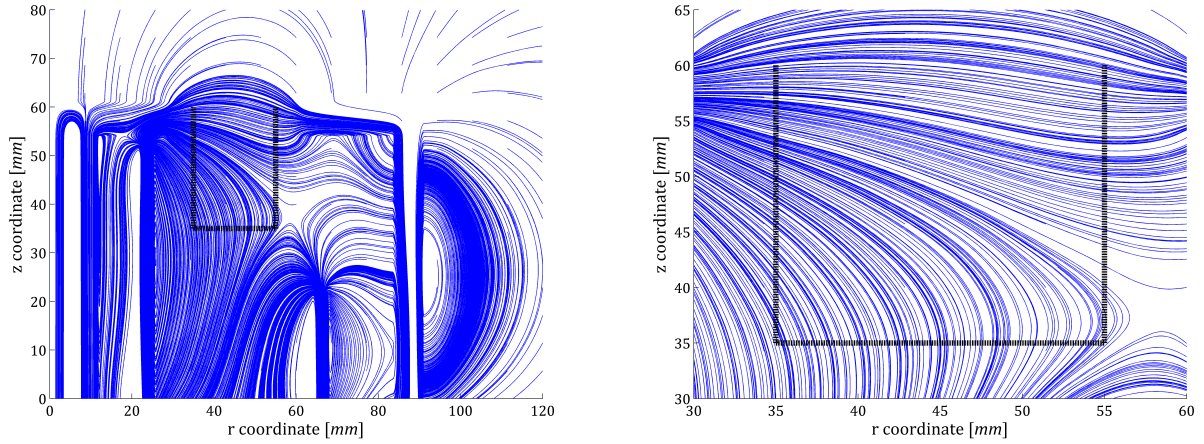

Figure 3.41: Streamlines suppressing the rear part of the magnetic shield and magnetic core. Right figure: zooming of the left one, focusing on the chamber region.

3.4.2 Different magnetic topologies

Up to this moment, the magnetic field topology found was as close as possible to the SPT 100 given by the EP2 group. During this section, different magnetic topologies of other thrusters such as the HEMP thrusters will be try to be reproduced within the configuration of the SPT 100 obtained in previous sections.

Magnetic topology of the HEMP thruster

The HEMP thruster is within the electrostatics acceleration of the ions as it is the case of Hall Effect Thrusters, but there are some differences between them.

Simulations performed by [14] demonstrated that the HEMP thuster allows for a high thermal efficiency because of the reduction and minimal energy dissipation and a high acceleration efficiency.
In the case of the HEMP the plasma only contact the wall in some limited areas of the magnetic cusps. For this reason, the erosion is been reduced with respect to the Hall Effect thrusters.
The magnetic field of the HEMP is formed by several cusps all along the chamber of the thruster. They are performed by means of magnet rings (see Figure 3.42).

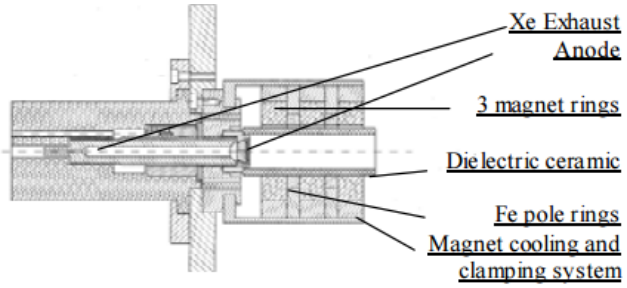

Figure 3.42: Scheme of a HEMP-T DM3a [15].

In order to emulate this topology of the magnetic field, the configuration presented at 3.43 will be followed. 3.42).

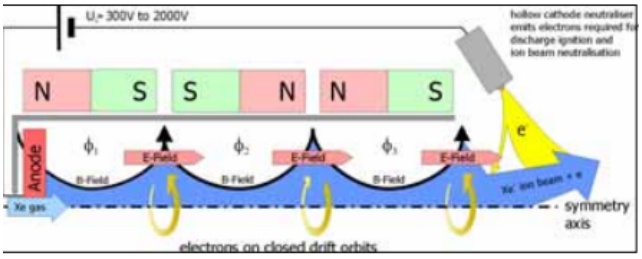

Figure 3.43: Scheme of the magnetic elements followed for the case of the SPT 100 thruster [15].

As a first approximation, magnetic elements are included. The material used is NdFeB37, the same one used in the magnetic shield. The distribution of them along the chamber of the thruster is presented at Figure 3.44. They are only distributed along the rear part of the chamber because close to the exit of the chamber the intensity of the magnetic field has a higher value and they do not present any change in streamlines when they are placed there. The configuration used is the same as Figure 3.43 NS, SN and NS, where N stands for the north and S is the south.

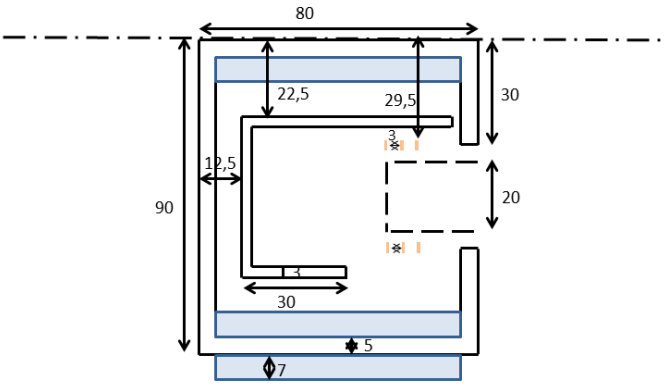

Figure 3.44: Scheme of the SPT 100 implemented with three magnet elements.

During these studies, streamlines are the only important parameters. Intensity of the magnetic field will not be considered.
Although the magnet elements are placed close to the position where the magnetic field have the lower values, those are not strong enough to form the desire shape in that area.

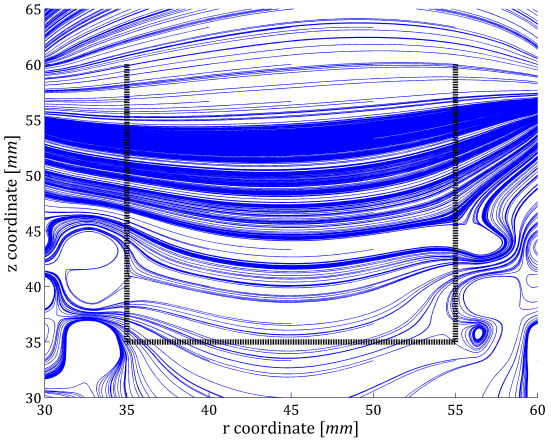

Figure 3.45: Streamlines inside the chamber when magnet elements are placed surrounding the chamber.

For that reason, they are going to be changed by solenoid elements in which the J parameter could be increased, besides the physical meaning, so as to have an influence on the streamlines inside the chamber.
The names of the different solenoids are presented at Figure 3.46.

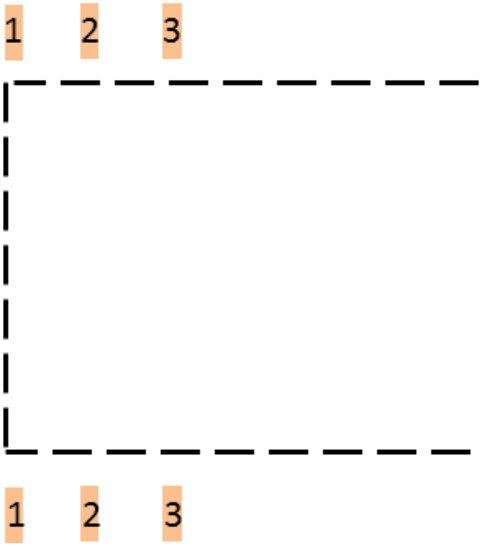

Figure 3.46: Names of the solenoids places along the chamber.

The characteristics of the solenoids used are presented at Table 3.5. As previosly mentioned, the values of the parameter J have no possble physical meaning in the solenoids used, as the size of them are small and the number of turns could no be satisfy in that reduced area.

Element	**Wiring parameters**
Solenoid 1	AWG12 (d = 2.053 mm) $J = 6300$ A · turns N = 700 turns
Solenoid 2	AWG12 (d = 2.053 mm) $J = 12600$ A · turns N = 1400 turns
Solenoid 3	AWG12 (d = 2.053 mm) $J = 6300$ A · turns N = 700 turns

Table 3.5: Characteristics of the solenoids sorrounding the chamber.

In the rear part of the chamber, the topology of the cusps could be found. There are two of them and this allows to reduce the erosion in that areas.

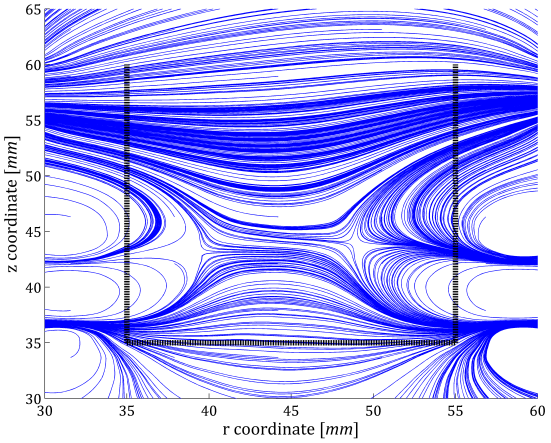

Figure 3.47: Streamlines inside the chamber when solenoids are placed surrounding the chamber.

Lens topology

Another interesting topology of the magnetic field is the lens one presented at Figure 3.48. This zero magnetic field region can be obtained by a supplementary coil positioned behind the chamber of the thruster.

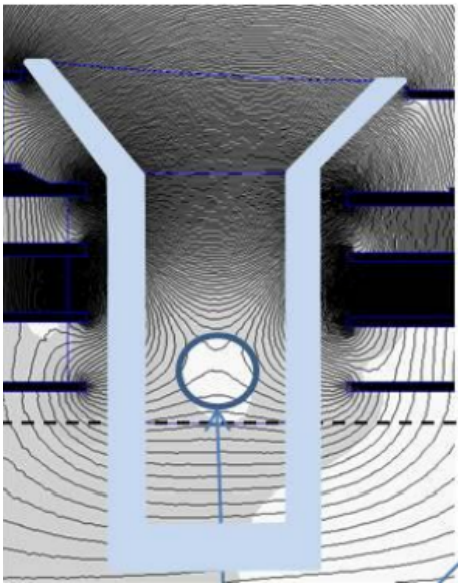

Figure 3.48: Cusps topology for the PPS-FLEX, a Hall Effect , when a solenoid is placed in the rear part of the chamber. [17]

In such a way, in the distribution of the SPT 100, a rear solenoid is included. The characteristics of it are presented at Table 3.6.

Element	**Wiring parameters**
Rear coil	AWG12 (d = 2.053 mm) $J = 3600$ A $\cdot$ turns N = 400 turns

Table 3.6: Characteristics of the rear coil located in the SPT 100.

The following results are obtained (Figure 3.49. The convex streamlines are not symmetric at r = 45 mm, they are displaced towards. Moreover along the wall chamber, a cusps shape is obtained. This is not as expected, for this reason this way of obtaining the lens topology will be not considered valid.

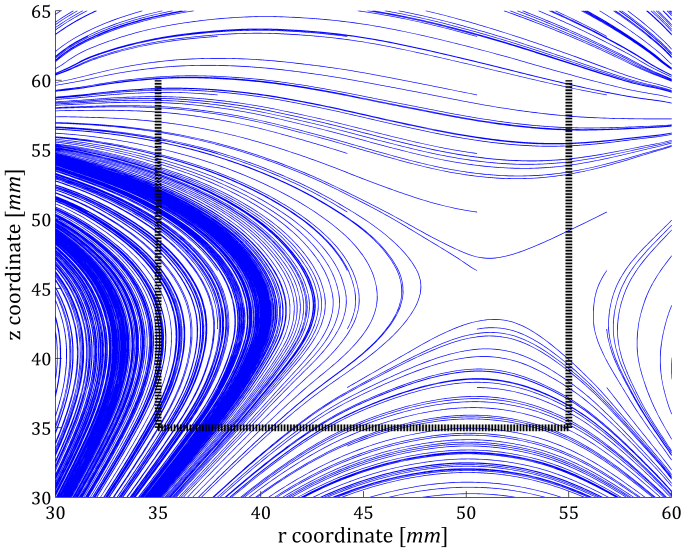

Figure 3.49: Cusps topology when a rear coil is placed in the rear part of the chamber.

The other way to achieve could be placed some magnets in the rear part of the chamber 3.50. Forcing them to have the appropriate magnet direction, streamlines in the rear part could be placed in that desired shape. The magnet position selected is pointing towards the axis of symmetry.

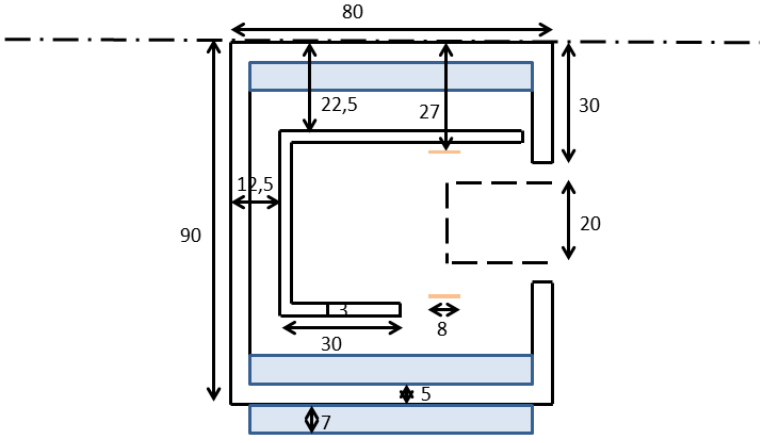

Figure 3.50: Scheme of the SPT 100 when the magnet are placed.

In this case, streamlines are more similar to the desired ones. There is a change in the concave/convex orientation of the lines as the z coordinate increases. The singular points are located outside of the chamber regime.

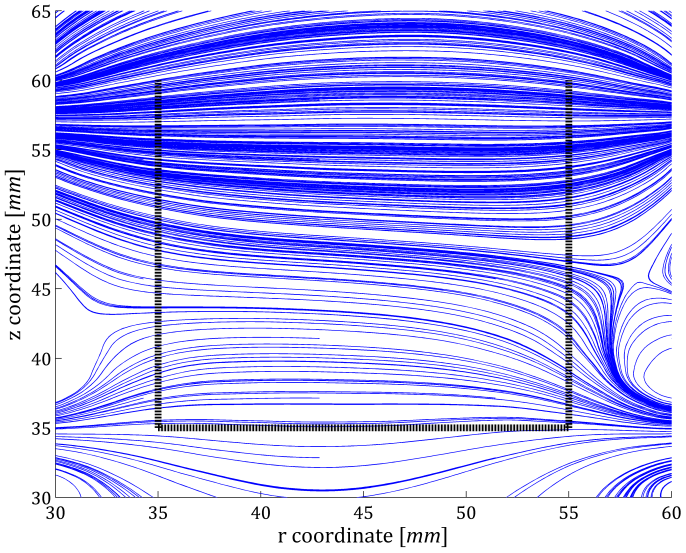

Figure 3.51: Cusps topology when two magnet are placed in the rear part of the chamber.

Chapter 4

Studies of the Helicon Plasma Thruster

This chapter will provide the reader with an analysis of the different electromagnets and magnets surrounding the chamber of a Helicon Plasma Thruster (HPT).
First, a selection of the different elements is going to be explained. Then, different studies regarding the diverse elements are going to be taken into consideration.
During this section the magnetic field dimensions will be Gauss (G), 1 T = 10^4 G.

4.1 Design of the HPT

The design of the HPT studied is been taken from the information given by EP2 as, together with Sener Company, they are studing a prototype of this type of thruster.
The final dimensions of the thuster implemented are L = 15 cm and R = 1,5 cm. The inner radius will be constant during the complete analysis, while the length will be changed in some studies as one of the advantages of this prototype is related to the capability of changing the length of the chamber.
The Helicon Plasma Thruster is composed by two solenoids (fore and after), whose main function is the generation of the magnetic field inside the chamber; and a nozzle coil in charge of the control on the magnetic nozzle. The nozzle coil current is independently controllable with respect to the solenoid ones.
Moreover, a permanent magnet is been considered for later studies.
The different parameters that characterize each of the element and its position will be shown at Table 4.1.
And, once again, the environment material used is air. The material used to wire solenoids is copper.
The scheme of the thruster implemented in the program is presented at Figure 1.2. The rectangles represent both solenoids and the nozzle coil, respectively, while the dashed line represent the location of the chamber of the thruster and the dotted-dashed line serves as the axis of revolution.
All the dimensions are presented in mm.

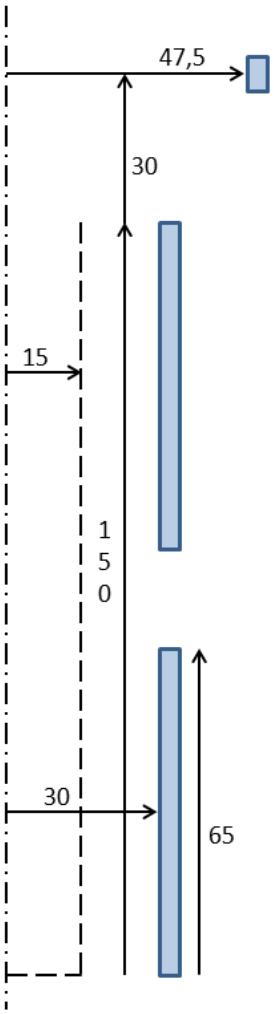

Figure 4.1: Dimensions of the HPT implemented. All the elements are enlarged as they are analyzed as punctual elements.

Element	**Wire parameters**
Solenoid	AWG12 (d = 2.053 mm) $J = 3789.3$ A · turns N = 434 turns
Nozzle coil	AWG10 (d = 2.558 mm) $J = 1894.6$ A · turns N = 143 turns

Table 4.1: Magnetic generators with their characteristics.

where $J = I \cdot N$ (I stands for the intensity and N number of turns) and d is the diameter of the wire used. All the magnetic elements used in this model have the magnetic lines in a counterclockwise direction.
The boundary conditions established far from the thruster and its magnetic elements are Dirichlet ones, meaning that far away from the thruster the potential is set equal to zero.
In a first analysis, all the magnetic elements are considered as a punctual objects with negligible mass. The

magnetic field distribution is presented at Figure 4.2. The black lines show the chamber of the thruster and the magnetic elements, respectively.
The high values of the magnetic field are because of the nozzle coil located close to that region. The magnetic field inside the chamber is mainly axial in the central region of the chamber whose values vary from 550 G where the solenoids are located and 330 G in the rear part of the chamber.

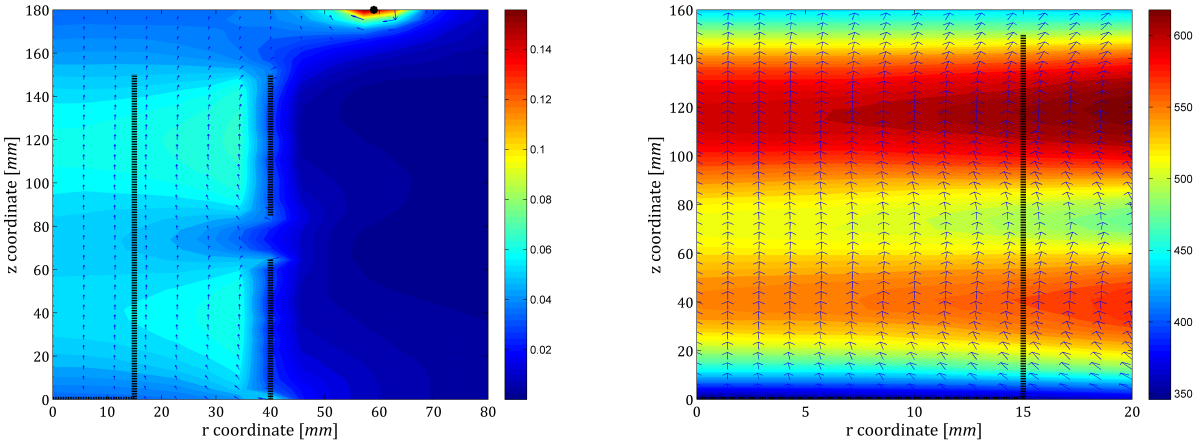

Figure 4.2: Magnetic field values for $L = 150mm$. Right figure: zooming of the left one, focusing on the chamber region.

4.2 Analysis of the Magnetic Elements

4.2.1 Filling Factor

In order to add more realistic values for the analysis of the magnetic field, the size of the elements will be increased and the filling factor (K_u) will be taken into consideration. This parameters is related to the space left once the wire is placed along the magnetic element (see Figure 4.3).

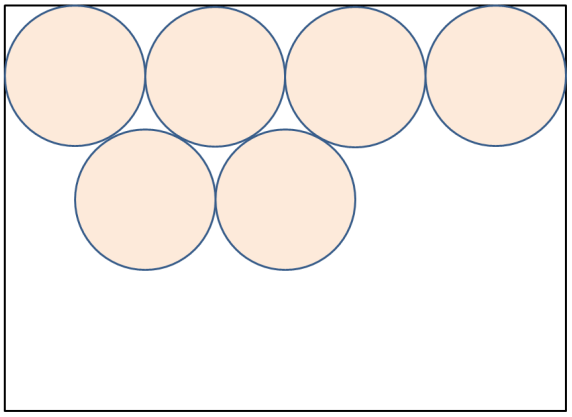

Figure 4.3: filling factor within the magnetic element.

In order to quantify those values, Equation 4.1 are going to be used.

$$K_u = \frac{V_{wire}}{V_{total}} = \frac{2\pi\bar{R}\frac{\pi d^2}{4}N}{2\pi\bar{R}hr_d} = \frac{\pi d^2 N}{4Lr_d} \tag{4.1}$$

where V_{wire} and V_{total} stand for the volume of the wire and solenoid/nozzle coil used. $\bar{R}$ is the mean radius of the magnetic element, d is the diameter of the wire used, N is the number of turns, L and r_d are the axial and radial dimensions of the magnetic element.
The value selected for the filling factor is an conservative one so as to correct all the possible errors could be considered. Some of those errors are related to the winding of the wire may not be a perfect hollow cylinder (it can have a slightly oval shape), the wire diameter may not be exact. And moreover, the windings may not form such a regular pattern and this will alter the ratio of wire volume/total volume.
Taking into account possible errors, the selected value for the filling factor is 0.4.
The equation 4.1 must be particularize for each of the different magnetic elements implemented. The only unknown of 4.1 is the radial length, so it is going to be calculated as a function of the filling factor.

$$r = \frac{\pi d^2 N}{4LK_u} \tag{4.2}$$

During this section, the filling factor function will vary from $[1 - 0.4]$. The values of the radial length as a function of K_u will be showed in table 4.2.

K_u	$rd[mm]$	OR [mm]
1	21.8	51.8
0.75	29.2	59.2
0.61	35.9	65.9
0.5	43.7	73.7
0.4	55.1	85.1

K_u	$rd[mm]$	OR [mm]
1	29.5	76.75
0.75	39.4	86.65
0.61	48.4	95.65
0.5	59.1	106.35
0.4	73.86	121.11

Table 4.2: Radial length for the selected K_u. Left table: solenoid. Right table: nozzle coil

where the OR stands for the outer radius and it is equal to $IR + r_d$.
Once all the dimensions are established, the magnetic field obtained in each of the values of the filling factor is going to be compared with the case of punctual magnetic elements (infinitive filling factor). The infinitive filling factor, for the case studied, is considered 19.
All the errors presented in this section are expressed in %.
When the reference case is compared with a $K_u = 1$, the higher difference occur near the rear part of the thruster (reaching a value of $\triangle B = -25$ G). The behavior of the difference seems as a symmetric one whose axis of symmetry is allocate around z = 75 mm. The error mainly varies from $[-3 : 1]$% in most of the places inside the chamber.

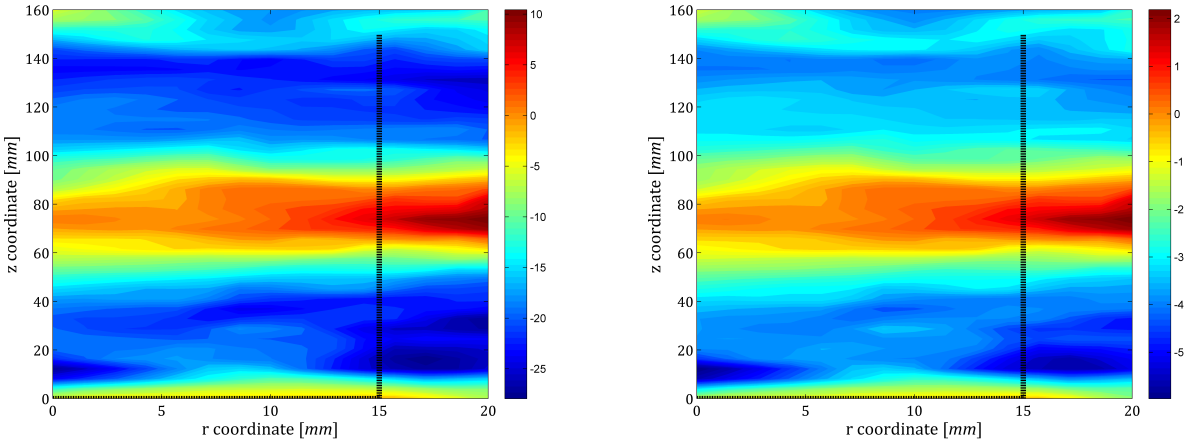

Figure 4.4: Comparison between $K_u \rightarrow$ inf and $K_u = 1$. Left figure represents the difference between magnetic values. Right figure represents the error of the magnetic element with respect to the reference one.

When comparing punctual elements with more real elements ($K_u = 0.75$, see Figure 4.5, $K_u = 0.61$, see Figure 4.6 and $K_u = 0.5$, see Figure 4.7), the behavior is the same explained with Figure 4.4. The higher the filling factor, the higher the difference in magnetic field and consequently the error is. This is because of the increased in size of all the magnetic elements placed around the chamber of the thruster and the increase of the intensity of the magnetic field. Moreover, the lower the filling factor, maximum values of the error are also presented at the exit if the chamber. For instance, for the lower filling factor $K_u = 0.5$, in which the maximum error is obtained compared with the rest of the filling factor used, the greatest error is -12% and it is located in the bottom part and close to the wall of the chamber and also close to the exit of the chamber.

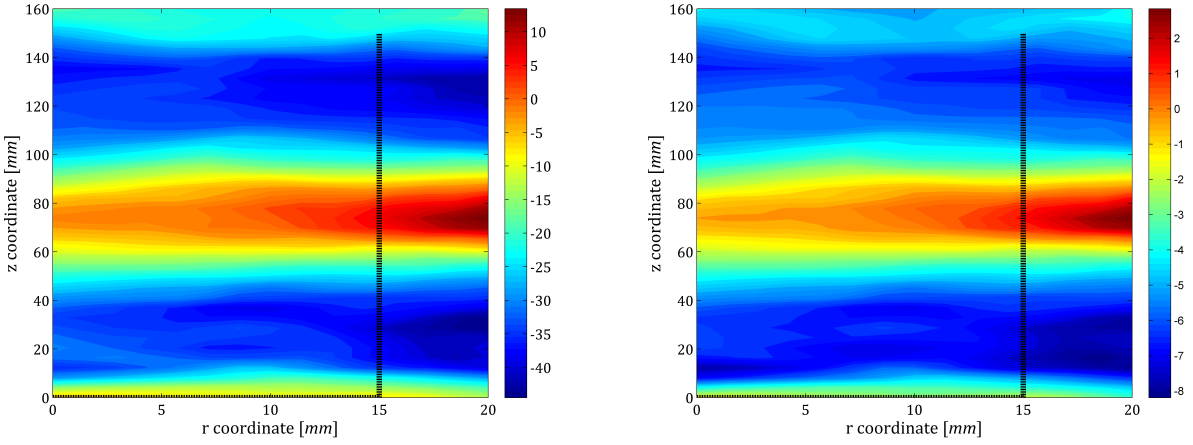

Figure 4.5: Comparison between $K_u \rightarrow$ inf and $K_u = 0.75$. Left figure represents the difference between magnetic values. Right figure represents the error of the magnetic element with respect to the reference one.

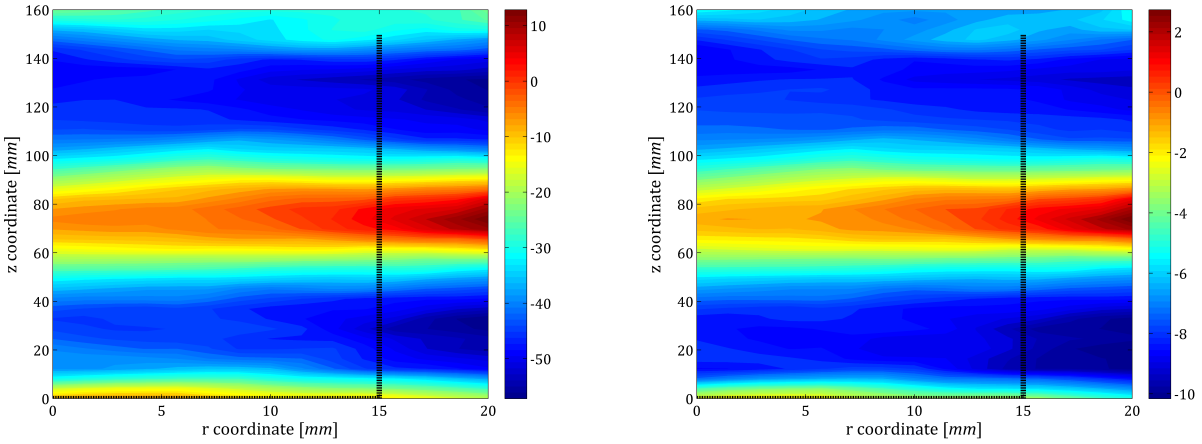

Figure 4.6: Comparison between $K_u \rightarrow$ inf and $K_u = 0.61$. Left figure represents the difference between magnetic values. Right figure represents the error of the magnetic element with respect to the reference one.

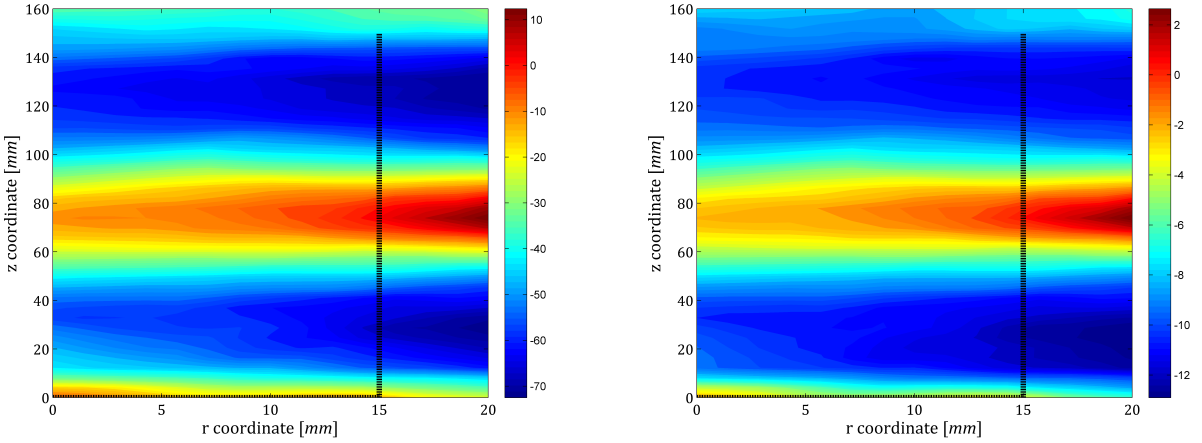

Figure 4.7: Comparison between $K_u \rightarrow$ inf and $K_u = 0.5$. Left figure represents the difference between magnetic values. Right figure represents the error of the magnetic element with respect to the reference one.

An special mention will be done to the case for $K_u = 0.4$ as this will be the case taken as reference in the following sections. The maximum error occurs close to $r = 15$ mm in the exit of the thruster. The maximum error is -11 %, what implies a change of -70 G.

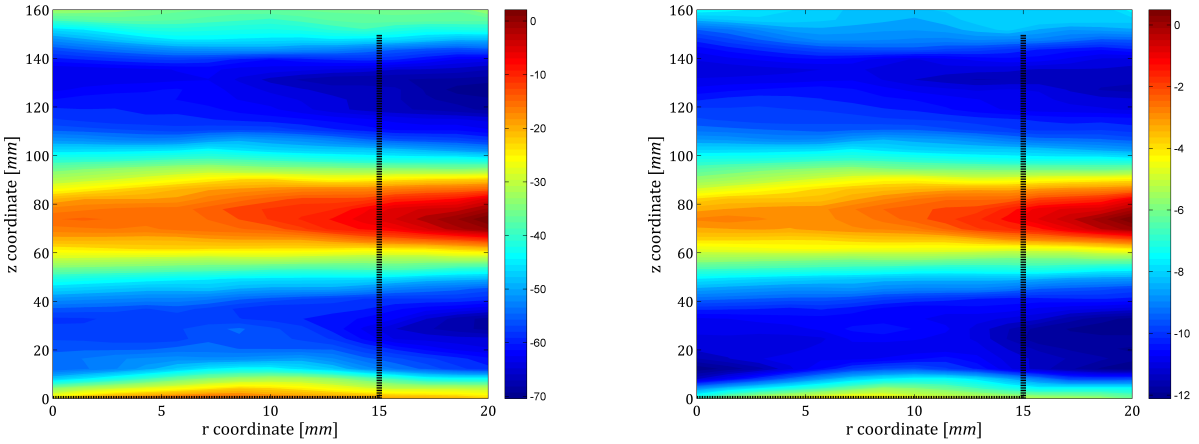

Figure 4.8: Comparison between $K_u \to$ inf and $K_u = 0.4$. Left figure represents the difference between magnetic values. Right figure represents the error of the magnetic element with respect to the reference one.

4.2.2 Changes in the length of the chamber

One of the advantages of this HPT used by the EP2 and Sener group is related to the possibility of changing the length of the chamber. The values selected for the analysis are between $[15 - 25]$ cm. The analysis of the magnetic field inside the chamber and the exterior region is going to be studied.

In all the cases, both solenoids and the nozzle coil are kept of constant size, just the relative position between solenoids will be changed. The selected filling factor factor $K_u = 0.4$ as it the conservative value for a circular sectional area as it is the case for the solenoids and the nozzle coil (as previously explained at 4.2.1).

The nozzle coil is kept at the initial location while the position of the solenoids changed from the middle region to the extreme ones with respect to the chamber length. An important fact that must be taken into consideration, when performing the middle location of the solenoids is related to the distance between them. The distance must be at least 2 cm in order to leave room for the antenna and the antenna feed needed in this kind of thrusters.

In order to compare the results of all the studied cases, the mean value of the magnetic just inside the chamber is going to be considered.

Three different values of the length chamber are implemented: 15, 20 and 25 cm. The minimum value is the minimum that can be selected because of the length of each of the solenoid and the minimum separation between them.

In the case of the middle location of the solenoids, the mean values follow an inverse linear relation. The higher the length, the lower the mean value (Figure 4.9). This is related to the homogeneity of the magnetic field inside the chamber (Figure 4.10). An increase of 10 % of the length, implies a decreased of 8,5 % of the mean value of the magnetic field.

For the case of located the solenoids in the extreme section, the mean value follows the same behavior, the higher the length the lower the mean value of the magnetic field, but in this case the relation is no longer linear. Once the chamber length is kept constant, the lower the distance between the solenoids, the greater the value of mean magnetic field. Taking a look at the maximum studied, the mean values can vary from 325 G to 385 G for the extreme and middle section, respectively, implying an increase of 17 %.

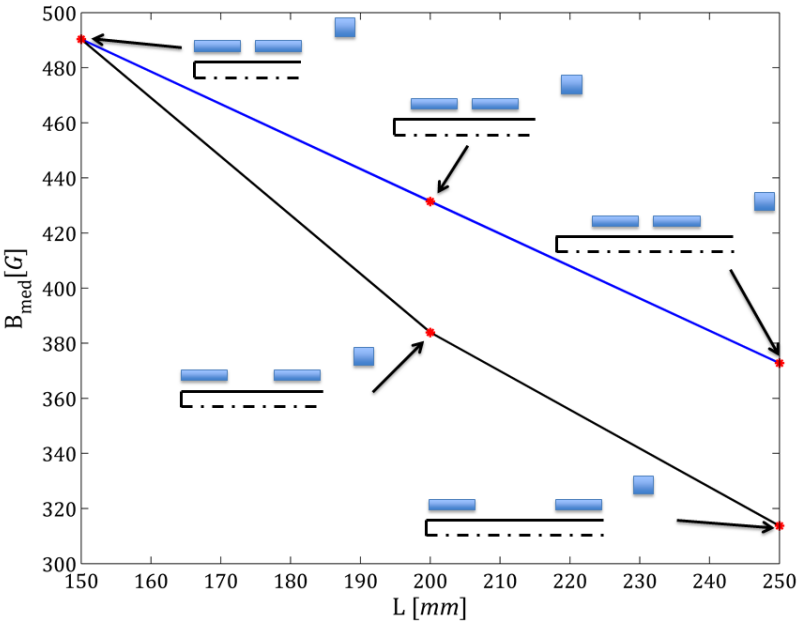

Figure 4.9: Evolution of the mean value of the magnetic field as a function of the chamber length. Blue line, solenoids are kept at the extremes; black line solenoids at the middle section.

As a theoretical pre-design of the HPT discharge-chamber realized by EP2 and Sener [18] which determines some properties (source size, magnetic strength, etc.) has been developed with respect to the results of plasma flow simulation of the thruster. These analysis have been guided with the simplified theory of RF waves magnetized cold uniform plasma. This theory determines parametric regions of the applied static magnetic field strength against plasma density and the static magnetic field obtained by EP2 and Sener is $B_0 = 450$ G. This value is inside the regime considered in the previous studied, when it varies from 490 G in the case of the smallest length and 315 G for the greatest one.
To analyze the homogeneity of the magnetic field inside the chamber, the error with respect to the mean value of the magnetic field will be taken into consideration.

$$\sigma(\%) = 100\frac{B(r,z) - B_{med}}{B_{med}} \tag{4.3}$$

where B(r,z) is the magnetic field in each of the different locations of the study and B_{med} is the mean value of the magnetic field just considering the chamber.
For the case of the case of $L = 150$ mm, (figure 4.10), the regions out of the chamber are out of the scope of the interest. Being focus on the deviation inside the chamber, there are some relevant differences comparing the exit and the rear part of the chamber. The variation of the magnetic field changes from 10% in the upper part of the chamber and, -30% in the lower part of the chamber. That important difference could be solved by adding an extra magnetic element in the rear part of the thruster in order to increase the value in that area.

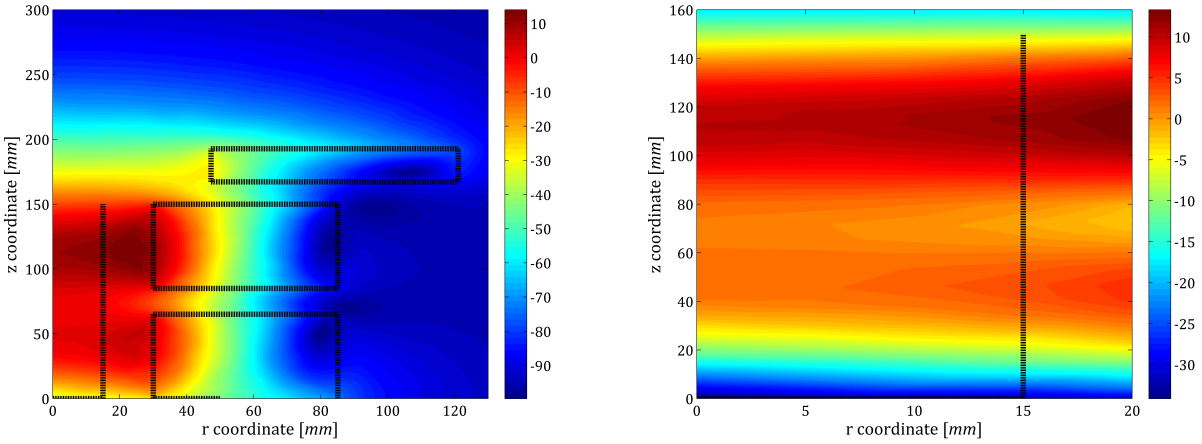

Figure 4.10: Magnetic field deviation for $L = 150$ mm. $B_{med} = 490$ G. Right figure: zooming of the left one, focusing on the chamber region.

Analyzing the $L = 200$ mm (figure 4.11) and $L = 250$ mm (figure 4.12) where the solenoids are located in the middle region, the same behavior as previously explained happened. This performance is even more evident as the length is been increased. For $L = 200$ mm, in the exit region, there is an error of -20 %. In addition to that, in the central section of the chamber the disparities vary from 20 % to 0 %. And, in the rear part, there is the peak of deviation reaching a value of -60%. As previously mention, this could be solved by adding a new magnet elements.
In the case of $L = 250$ mm, the peak reaches a value of -70% in the rear part and 30% to 0 % in the central region. Moreover, when the error -40 % in the exit of the chamber.
All these behavior, in which in the rear and exit regions the deviation obtained have negative values, and in the central ones varies from positive values to zero ones are related to the location of the solenoids and the mean value obtained.

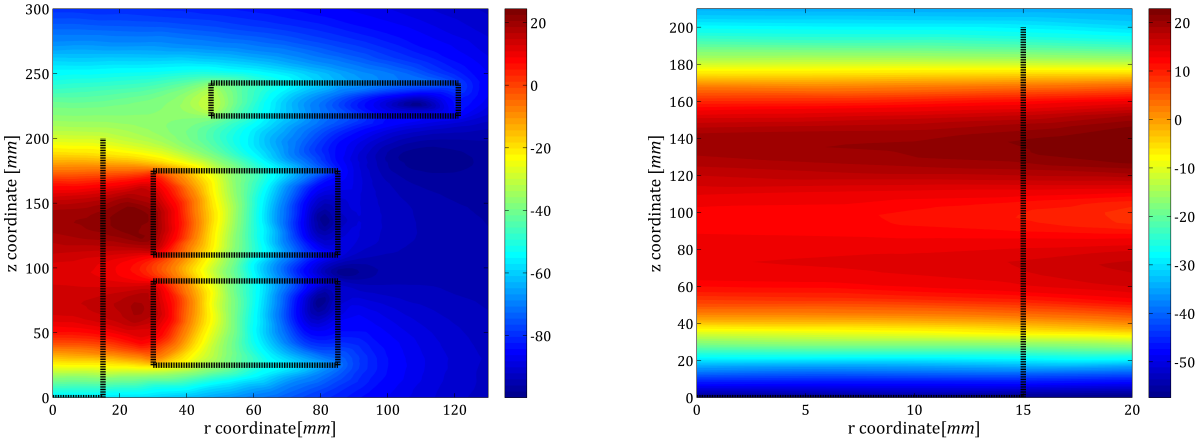

Figure 4.11: Magnetic field deviation for $L = 200$ mm. $B_{med} = 432$ G. Right figure: zooming of the left one, focusing on the chamber region.

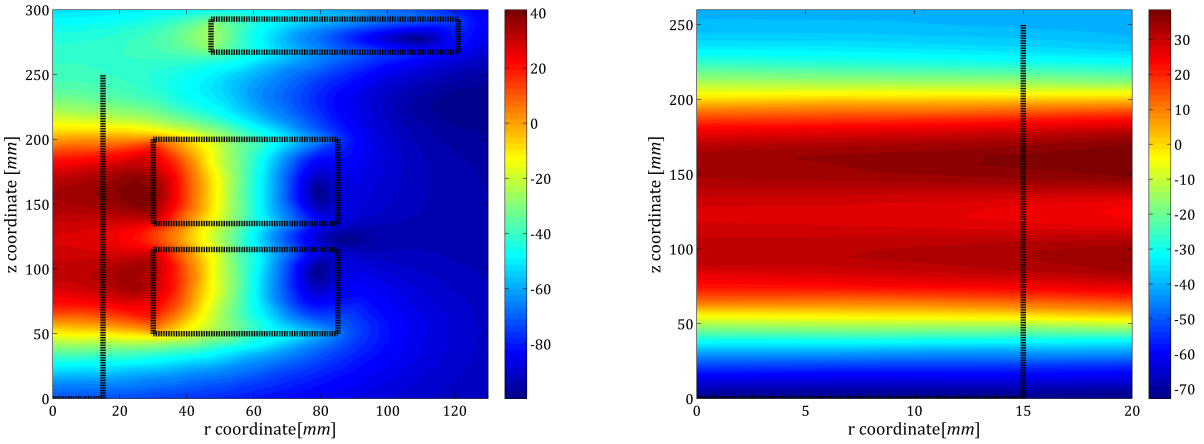

Figure 4.12: Magnetic field deviation for $L = 250mm$. $B_{med} = 373G$. Right figure: zooming of the left one, focusing on the chamber region.

When the solenoids are located in the extremes of the chamber, in both cases, for $L = 200$ mm (figure 4.13) and $L = 250$ mm (figure 4.14). The changes occur all along the chamber. But there is an important difference between the position were the solenoids are located are where they are not. The error close to the solenoids location are positive ones, while in the middle region (where they are not) the error is negative. This is related to the magnetic field of the different points. In the middle section the magnetic field is lower than the mean one, while in the extreme locations (rear and exit) the value is higher.
In addition to that, the higher the length of the chamber, the higher the disparity is becuase of the higher distance between solenoids.

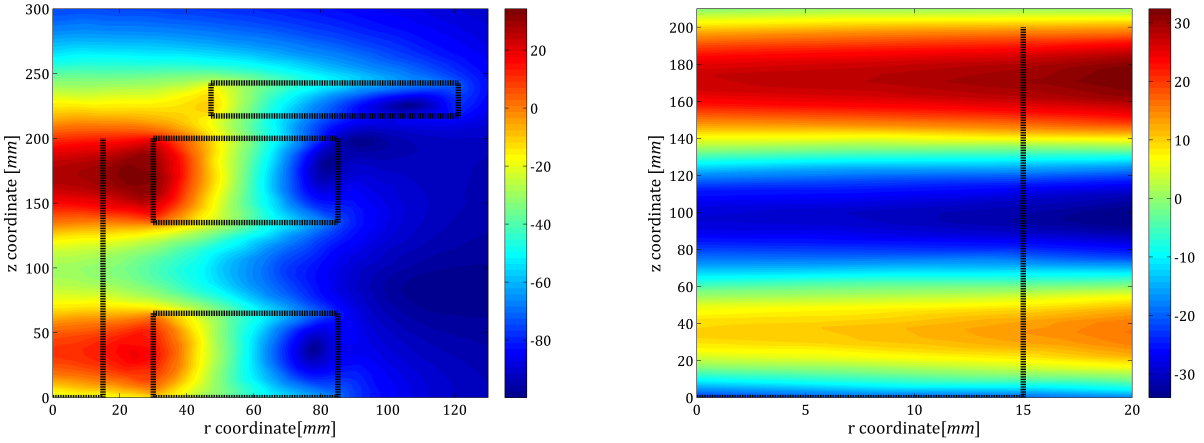

Figure 4.13: Magnetic field deviation for $L = 200mm$. $B_{med} = 371G$. Right figure: zooming of the left one, focusing on the chamber region.

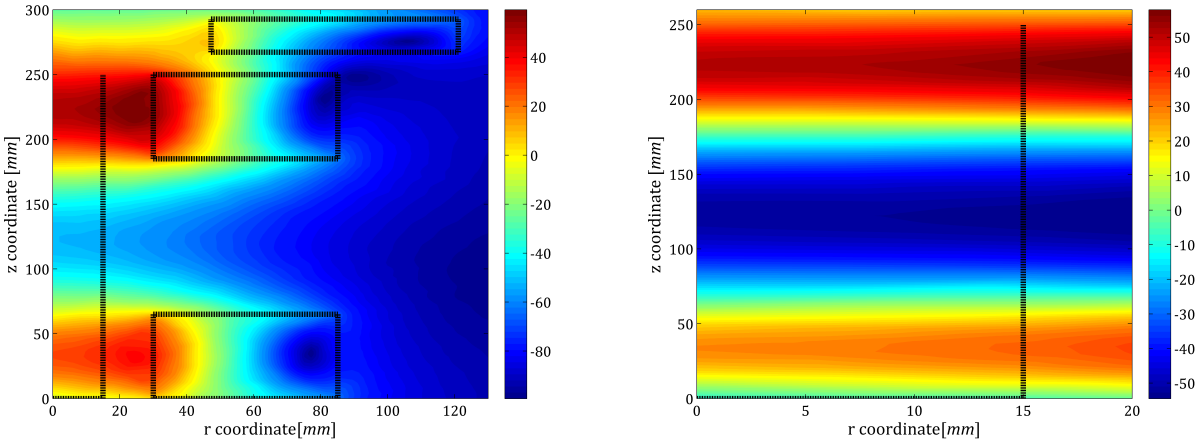

Figure 4.14: Magnetic field deviation for $L = 250mm$. $B_{med} = 314G$. Right figure: zooming of the left one, focusing on the chamber region.

To summarize, the location of the solenoids affect the homogeneity of the HPT and the location of the higher disparities with respect to the mean value.
In every case, the changes of the magnetic field with respect to the reference one could be avoided by means of adding extra magnetic elements or changing the size of the used ones, but this fact have an effect on the mass of the thruster, and of course, this is an important parameter when talking about thrusters used in aerospace field.

Validation of the results

During the complete analysis, finite element method is been used. And as it was explained at Section 2, the problem is divided forming a mesh. In order to validate the mesh implemented, the values of the mean magnetic field inside the chamber are going to be studied.
The number of nodes are established by means of the mesh size. In a first approach (and the maximum size allow by FEMM 4.2.), the mesh size is 1 and it turns out that the number of nodes is 5614. The second analysis is performed with a mesh size of 0.9, and the number of nodes reaches a value of 18465.

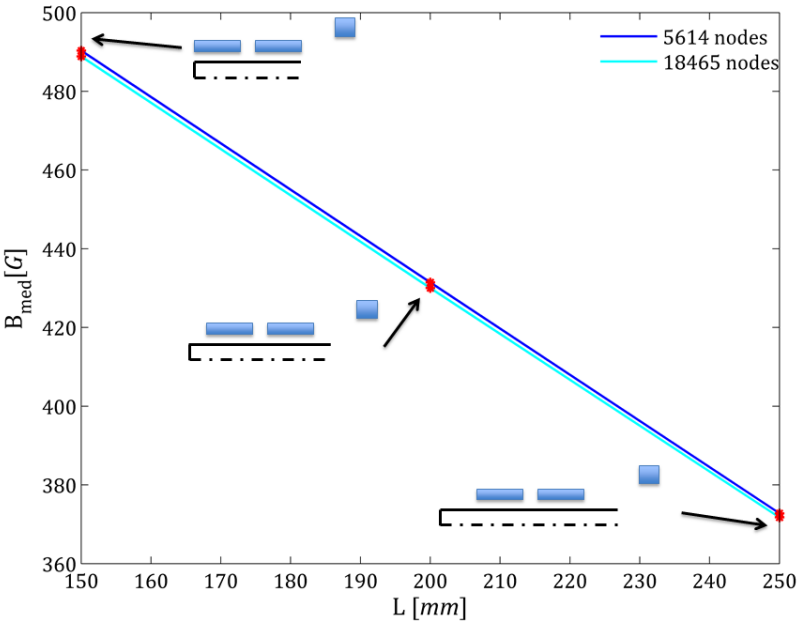

Figure 4.15: Validation of the results obtained as a function of the nodes used.

The difference between both analysis given in terms of % and setting as the reference value of one with the smallest number of nodes is presented at table 4.3.

Length [mm]	B_{med} **difference** [%]
150	0.298
200	0.334
250	0.288

Table 4.3: Difference in the mean value of the magnetic field when changing the mesh size

The variation between those values is less than 1%, so the mesh size used (mesh size = 1) can be implemented in order to have accurate enough results.

4.2.3 Analysis of the Nozzle Coil

Besides in previous section, the studied is been focused on the chamber region, this part will be devoted mainly to the exit of the thruster and the magnetic nozzle region.
In this analysis, the length of the thruster studied is $L = 15$ cm and the solenoids will be kept constant in size and all the parameters such as J. On the other hand, the nozzle coil will be constant in size but a relevant parameter, J ($J = IN$), will be changed.

Ampere-turns problem

The J parameter is affected by the intensity that crosses the wire and the number of turns of wire that the nozzle coil, in this case, has. So, a brief study in a simple problem will be perform so as to know the different behavior of those specifications.
The problem will be executed with a solenoid located in an air environment. The middle point of the magnetic element is located at $(36, 137, 5)$. The IR is equal to 35 mm and its length is 5 mm. The wire used is cooper

with 18AWG properties whose diameter is $d = 1.19$ mm. The ampere-turn used is equal to 1000 $A \cdot turns$. In the Figure 4.16 the magnetic field intensity far from the solenoid is approaching to zero as the distance from the it increases. Close to the magnetic element, the highest value found is 950 G.

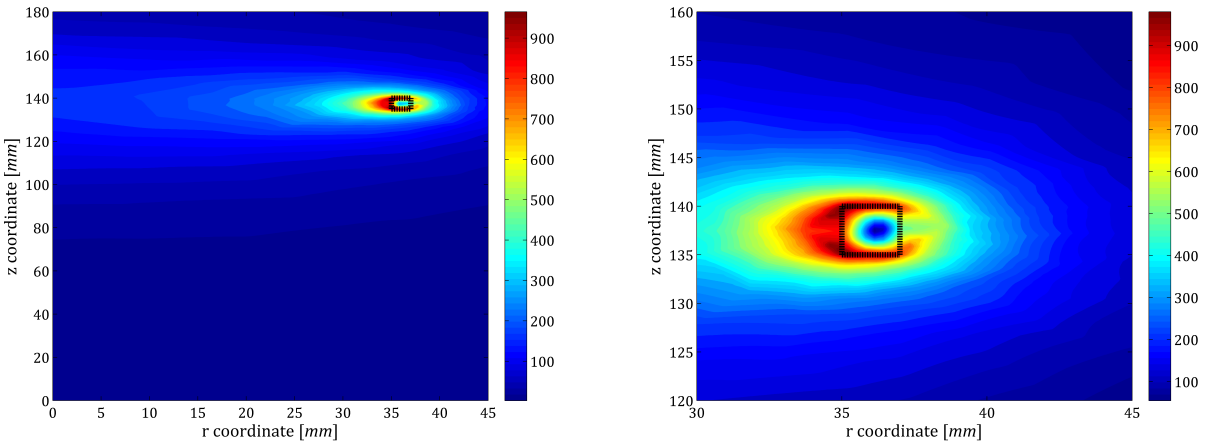

Figure 4.16: Magnetic field of a solenoid with $J = 1000A \cdot turns$. Right figure: zoom of the left one.

To continue with the analysis, the number of turns of the solenoid is changed. The study will be focused on the behavior close to the solenoid, in this way, just the zoom part will be represented in the following images. In the left figure 4.17, the number of turns is been decreased by a factor of 10, what implies that the magnetic field intensity is reduced by this quantity. In a similar way, when the number of turns is increased by a factor of 10, the intensity of the magnetic field also does (as it happens in the right figure 4.17). The shape of the magnetic field is kept the same. Summarizing, changing the number of turns and keeping the intensity constant, the shape of the magnetic field remains the same, while the intensity changes by the same factor as the number of turns is varied.

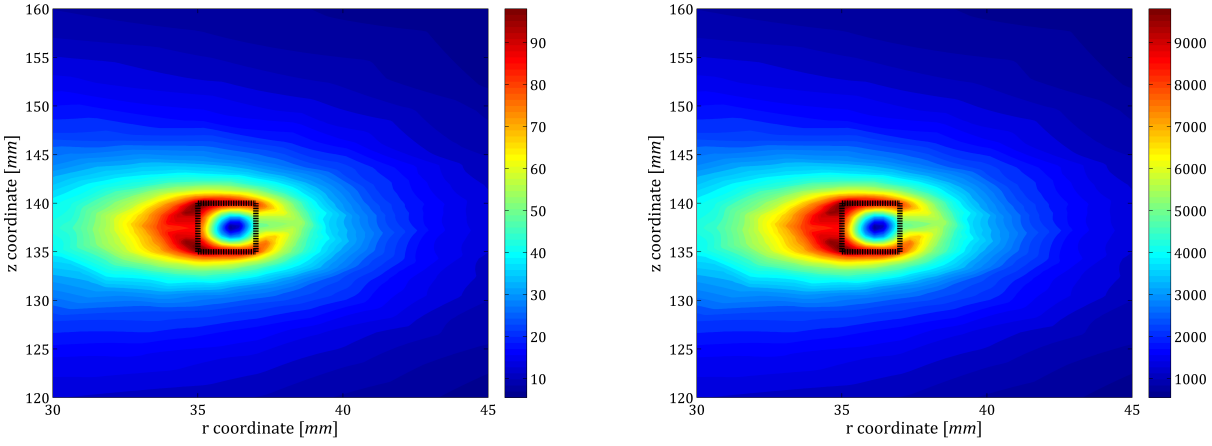

Figure 4.17: Magnetic field of a solenoid changing the number of turns. Left figure: $J = 100$ A $\cdot turns$. Right figure: $J = 1000$ A $\cdot turns$

The other parameter that can be changed in order to change J is the intensity. This analysis will be perform in the same manner as the number of turns, the intensity will be divided and multiplied by a factor of 10, and at the same time that the number of turns is kept constant. They follow the same behavior as the in the previous analysis; the shape remains the same while the intensity is been changed by the same factor as the intensity.

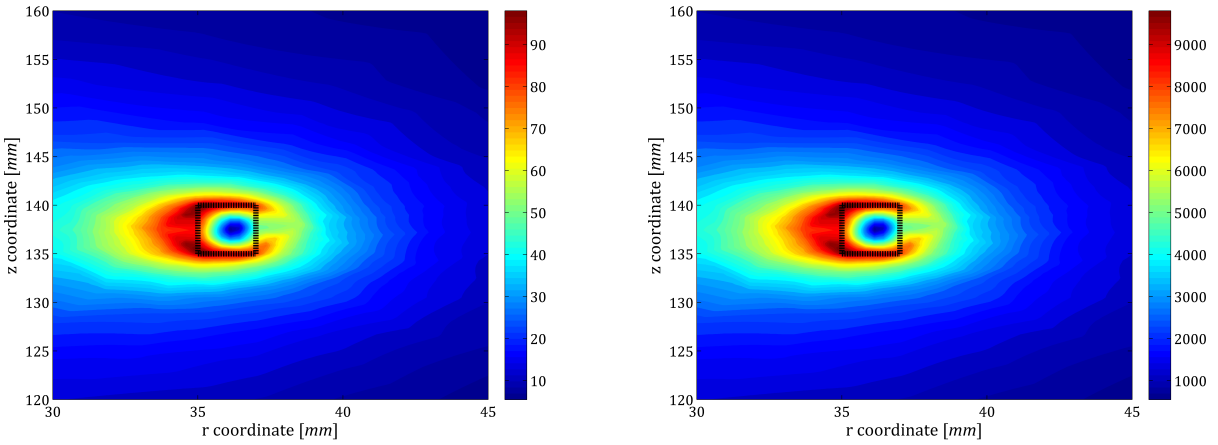

Figure 4.18: Magnetic field of a solenoid changing the intensity. Left figure: $J = 100A \cdot turns$. Right figure: $J = 1000A \cdot turns$

Summing up the results obtained, while the ampere-turn parameter change (no matter if the intensity or the number of turns does) the shape of the magnetic field is kept constant, and the intensity of the magnetic field changes in the same manner as the J does.
Going back to the main study of the Helicon Plasma Thruster, in order to change the ampere-turn parameter, the intensity will be changed while the number of turns is kept constant. The reason for that is related to the filling factor. This parameter is affected by the number of turns but it is not by the intensity, in that way, the size and the K_u remains, both, the same as it have been during the complete previous analysis.
In order to do so, the intensity is divided by two and doubled in two different studies.
In a first study, the point of interest will be limited to the exit of the thruster (r = 15 cm), and several points along that line are studied. The selected one are r = 5,10,15 mm. In the case of the intensity of the magnetic field, it follows a linear relation when the J parameter changes. But the relation is noyt as expected, if the intensity doubles, the intensity does not double, this is because, opposite to the simple case studied, there are more magnetic elements such as the solenoids that have also an influence in the intensity. Moreover, no matter where the point selected is, the intensity follows the same behavior.
In the case of the angle γ (see equation 4.4), the closer the point is to the symmetric line, the lower is the influence on the angle. And, the other way around for the point located nearer from the wall of the chamber has a higher influence. This is due to the position of the nozzle coil, as it is close to the wall, the influence in the angle is greater.

$$\gamma = \frac{B_r(r,z)}{B(r,z)} \tag{4.4}$$

where B_r is the radial magnetic field and B is the modulus of the magnetic field.

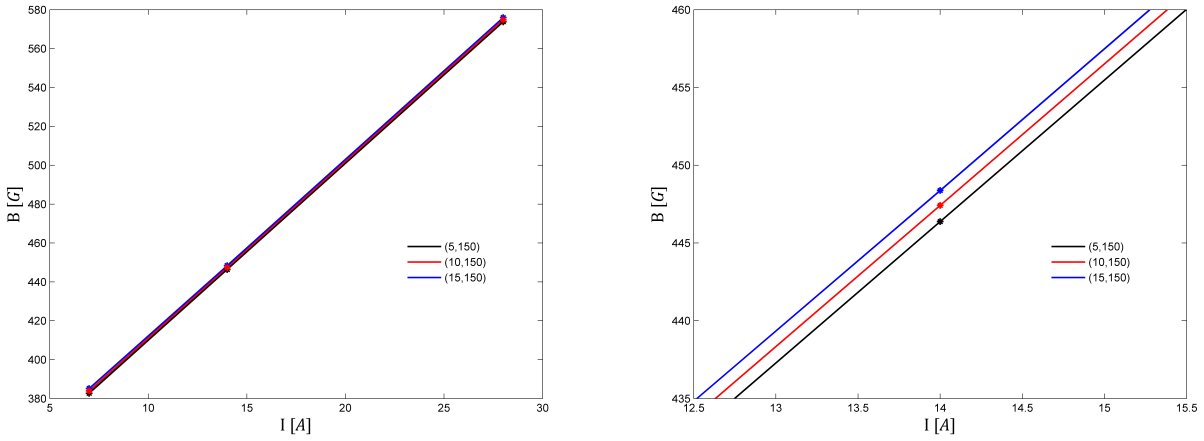

Figure 4.19: Magnetic field intensity selected in the exit of the thruster when changing the J parameter. Right figure: zoom from the left figure

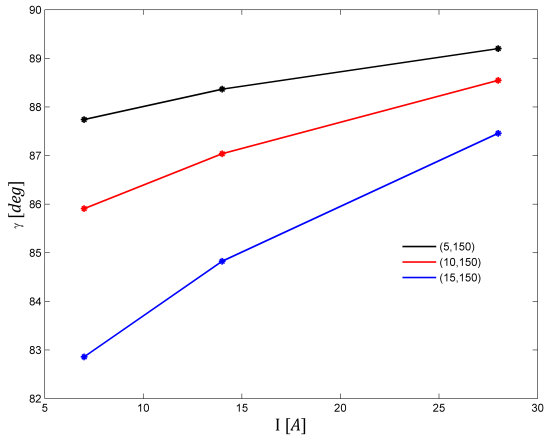

Figure 4.20: Angle (γ) selected in the exit of the thruster when changing the J parameter

Analyzing points located in the magnetic nozzle of the thruster, i.e. $z = 200$ mm, the results differ from the ones situated in the exit of the chamber. The increase/decrease of the intensity of the magnetic field depends how close/far is the point with respect to the symmetric line.
For the case of the angle, the influence of the position is not as significant as in the previous analysis. And in the case of the intensity of the magnetic field the relation is no longer linear.

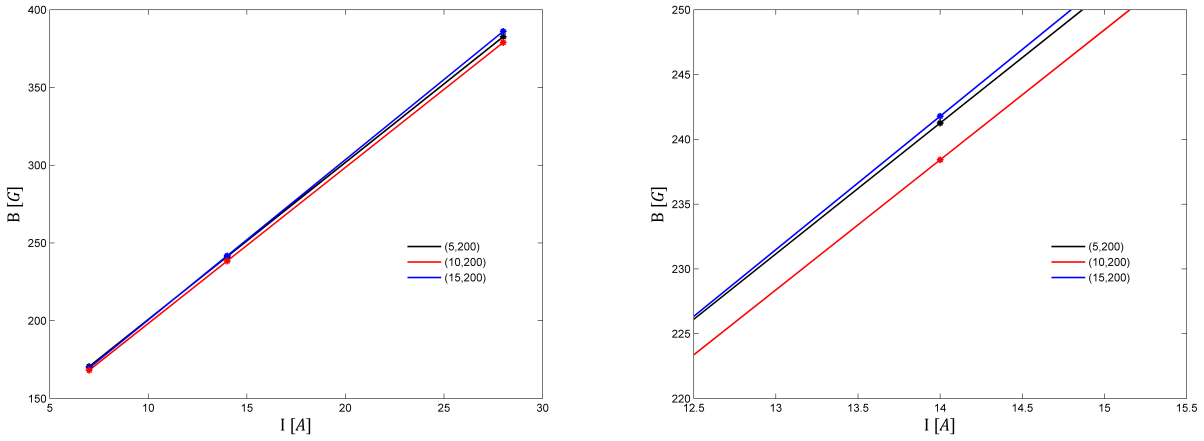

Figure 4.21: Magnetic field intensity selected in the nozzle of the thruster when changing the J parameter. Right figure: zoom from the left figure

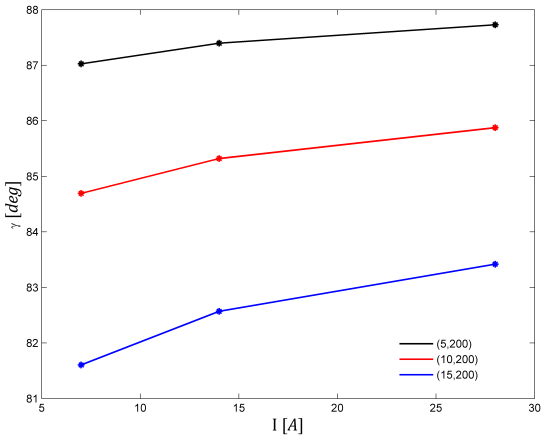

Figure 4.22: Angle (γ) selected in the nozzle of the thruster when changing the J parameter

Summarizing, when a change in the J of the nozzle coil is studied, the behavior of the intensity and angle of the magnetic field depends on where the point is located. When the point is in the exit of the thruster, the change in the intensity is independent on the r-coordinate, while the angle is highly influenced. If the position of interest is in the nozzle, both the intensity and the angle depends on the r-coordinate.

4.2.4 Addition of a Permanent Magnet

Up to this point, the analysis of the Helicon Plasma Thruster has been performed without the use of a permanent magnet at any location around the chamber. In this section, it will be introduced and a study taken into account different positions with it will be realized.

The permanent magnet is placed on the rear part of the chamber and it provides a magnetic shielding that helps to reduce the wall losses, and consequently, erosion in those walls that provokes the reduction of the life of the thruster, and contamination in the chamber of the thruster which produces efficiency losses.

The material of the permanent magnet NdFeB32, with radial magnetization, and it points towards the symmetric line (meaning that the magnetic lines go out from the side closer to the symmetric line).
The location of the reference magnet is 13 mm far from the rear wall of the thruster. Its inner radius is equal to 7 mm, the outer radius equal to 10 and its length is 10 mm.
During the following studies realized, an important parameter B_2/B_1 is taken into consideration. The B_2 stands for the intensity of a magnetic field located near the rear part of the thruster, and B_1 is the intensity of the magnetic field close to the exit (or at exit) of the thruster. This value, as explained before, should be as great as possible in order to avoid wall losses of the rear wall of the thruster (see [22] for further information).
The selected points are B_2 place along the $z = 0$ mm and B_1 at $z = 15$ cm. And all of them are placed at $r = 5, 10, 15$ mm. The most relevant ones are $r = 5, 10mm$ because in the case of the $r = 15$ mm, the ratio is even below 1 because of the influence of the nozzle coil place close to the exit of the thruster.
The first studied is performed varying the outer radius. The inner radius is always constant. The analysis is performed doubling, and multiplying by four the reference radial length of the thruster ($r_d = OR - IR$).
When the point is close to the axis of symmetry ($r = 5mm$), the increase in the radial length produces a linear increase in the ratio B_2/B_1. As the r dimension increases, the ratio behaves in a different manner. The greater increased in the ratio is produced, when the radial length is multiplied by 2. This is related to the higher size of the permanent magnet, and consequently, the higher values of the magnetic field close to the rear part.

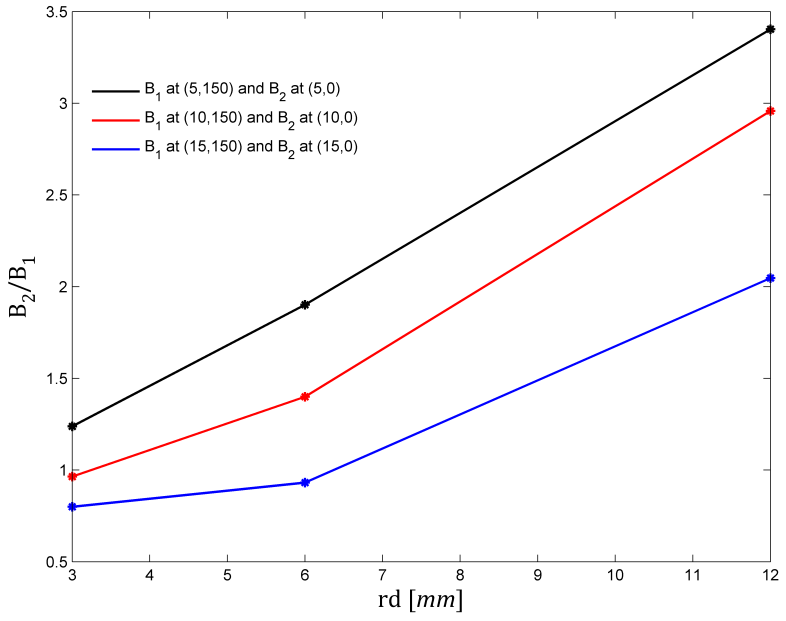

Figure 4.23: Magnetic ratio when changing the outer radius

The second studied is referred to the distance from the up line of the magnet to the rear part of the thruster. In this case, the distance is divided by two, double, and multiply by four. There is no minimum distance between the rear part and the magnetic element as it was the case of the solenoids.
In this case, the ratio decreases as the distance increases. This is because as the magnet gets farther from the rear part, the effect of increasing the intensity of the magnetic field in that part is reduced. When the distance is sufficiently high ($h = 25$ mm), the effect of the this distance been increased does not affect the relevant ratio.

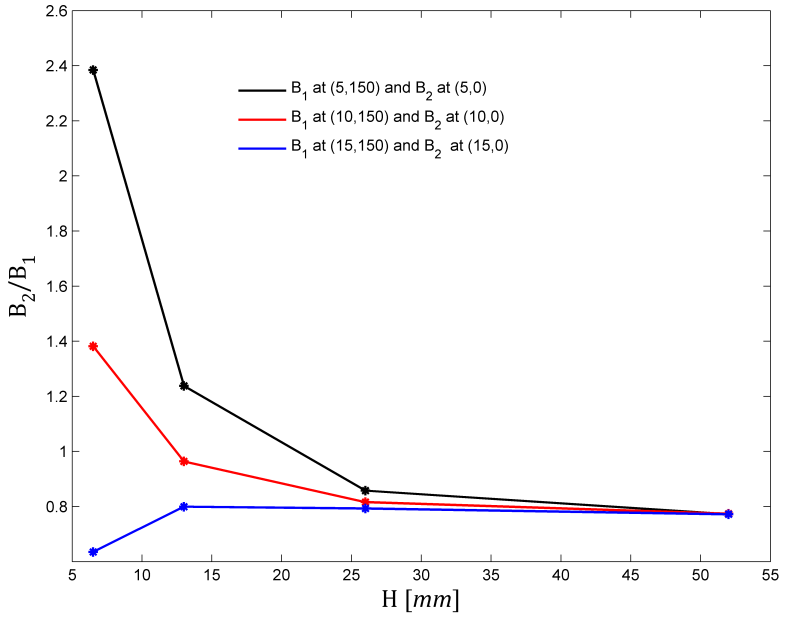

Figure 4.24: Magnetic ratio when changing the distance to the rear part of the chamber

The last studied is related to the length of the permanent magnet (Figure 4.25). Once again, this distance is doubled and multiplied by four. This analysis is the one which has less influence in the ratio B_2/B_1, it only produces an increase of 8% when $r = 5$ mm. Moreover, if the r = 15 mm line is not taken into consideration as B_2/B_1 is lower than 1 due to the proximity of the nozzle coil, there is no influence in the radial coordinate, as the behavior of the black and red lines is similar.

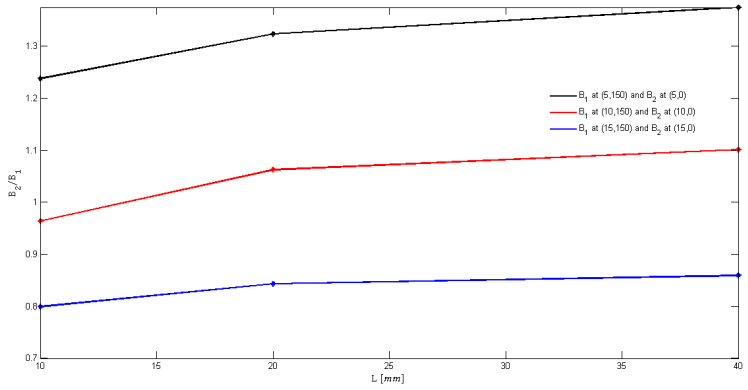

Figure 4.25: Magnetic ratio when changing the length

Chapter 5

Budget

The project is an theoretical one, for such a reason, there is no need of any kind of materials, except for the computer and the programs used. As it was said in 2.2, the main program needed FEMM 4.2. is a free licence one, so this will not add extra money to the project. Therefore, an estimation of the cost is presented at Table 5.1.

Uses	€
Engineering cost	10000
Matlab program	157
Computer use	67
Total cost	**10224**

Table 5.1: Budget needed in order to elaborate this project

The hours invested to perform this current project are 400, and the price per each work hour is 25 €.
The price for complete version of the Matlab program is 377. € with all the extra packages (see [23] for further information).

$$Matlabcost = 377€\frac{5months}{12months} = 157€ \tag{5.1}$$

where 5 months is the time required to performed the thesis.
The computer cost is related to the amortization of it. Assuming that it will not be sell once the lifetime is spent, the cost is calculated by the equation 5.2 (see [24]).

$$Computercost = 800€\frac{5months}{5years \cdot 12months/year} = 67€ \tag{5.2}$$

Chapter 6

Conclusions and Future works

The project developed for this thesis has as main objective the analysis of the magnetic field topology and intensity in different electric propulsion thrusters. This would not be possible without the aid of the finite element method. This practice allows to calculate accurate results in a short period of time, and allowing to analyze an important amount of different configurations without requiring the unaffordable cost of manufacturing all the prototypes.

The FEM program used in this thesis is FEMM 4.2., this is one of the most used programs to simulate simple magnetic circuits since it is an Open source code, and thus free to use. It is a relatively simple program and it is really fast realizing static problems, as it is the case of this project.

One of the advantages of the program used is related to the no limitation of the nodes that can be set. This permits to calculate really accurate results by means of increasing the number of nodes and elements used. In addition the code allows to use a wide range of elements in the magnetic circuit. The program enables the introduction of all kind of magnetic elements, and they are no longer punctual (the effect of the volume ratio can be analyzed). Moreover, the problem could be linked with Matlab/Octave program which support the possibility of postprocessing the result in a easy and powerful way. Furthermore, it allows to change properties with a specified code such as the material, or the size of the element, thus allowing to run parametric studies directly from Matlab becoming in this way a powerful tool for the design of magnetic circuits.

Although the program has some relevant advantages, it presents also some limitations. The program limits the analysis to planar or symmetric problems, excluding the 3D problems. Moreover, it is a basic problem in which some important properties such as the filling factor of coils and solenoids could not be taken into consideration when running the program.

Besides these disadvantages, problems analyzed in this thesis could be approximated to axisymmetric problem and they could be solved by means of FEMM 4.2.

Regarding the Hall Effect Thrusters, during this project an approximate magnetic circuit that reproduces the expected magnetic topology could be found with trial and error method. Moreover, some parametric studies have been performed and they allow to have a better idea of this kind of thrusters and they magnetic topology inside the chamber. Moreover, topology of other thrusters such as the HEMP type, having several Cups inside the chamber, has been reproduced so as to understand which are the differences on required in the circuit.

In the case of the Helicon Plasma Thrusters, studies were based on changing the different magnetic elements as well as the length of the chamber of the thruster to study the different behavior and intensity of the magnetic field inside the chamber and in the nozzle region depending on the examined case.

The current project has been considered as a starting point for future projects related to magnetic field in

different thrusters that could be focused on the development of optimization algorithms for the magnetic field topology.
As previously mention the code could be used if a axisymmetric configuration can be applied, otherwise a 3D code could be needed.
Moreover, this project was focused on the different magnetic topologies inside the chamber and the nozzle. Physical meaning and the behaviour of ions within this magnetic field could be also be included in future projects.

Bibliography

[1] Dan M. Goebel and Ira Katz.*Fundamentals of Electric Propulsion: Ion and Hall Thrusters*. Journal of Propulsion and Power,2004.

[2] E.Y. Choueiri.*A critical history of electric propulsion: The first 50 years (1906-1956)*. Journal of Propulsion and Power,2004.

[3] F.F. Chen and C.D. Decker.*Electron acceleration in helicon sources. Plasma physics and controlled fusion.* 1992.

[4] John Doe.*Hall Effect Thruster*. 2011.

[5] J. Navarro-Cavallé, M. Merino, E. Ahedo, M. Ruiz, V. Gómez and J.A. Gonzalez.*Helicon Plasma Thrusters: prototypes and advances on modeling*

[6] Steven A. Feuerborn, David A. Neary and Julie M. Perkins. *Finding a way: Boeing's "All Electric Propulsion Satellite"*, 2013.

[7] *EP2 web site* www.aero.uc3m.es/ep2 Consultation year: 2015

[8] David Meeker *Finite Element Method Magnetics. Version 4.2. User's Manual*, 2009.

[9] David Meeker *Finite Element Method Magnetics: OctaveFEMM. Version 4.2. User's Manual*, 2010.

[10] R. Sanjurjo, E. Lázara and P. de Miguel *Teoría de Circuitos Electricos*, 1997.

[11] J.M. Gallardo and F.I. Parra *Propulsión Espacial Eléctrica, Desarrollo de un motor de plasma de Efecto Hall*, 20.

[12] John A. Hamley, Gerald M. Hill and John M. Sankovic *Power electronics development for the SPT 100 thruster*, Ohio.

[13] J.R. Reitz, F.J. Milford, and R.W.Christy *Fundamentos de la teoría electromagnética*, 1996.

[14] K. Matyash, R. Schneider, A. Mutzke and O. Kalentev *Comparison of SPT and HEMP thruster concepts from kinetic simulations*, 2009.

[15] Günter Kornfeld, Norbert Koch. and Hans-Peter Harmann *Physics and Evolution of HEMP-Thrusters*, 2007.

[16] Daniel Perez, Pablo Fajardo and Eduardo Ahedo *Evaluation of Erosion Reduction Mechanisms in Hall Effect Thrusters*, 2015.

[17] C. Henaux, R. Vilamot1, L. Garrigues and D.Harribey *A new flexible magnetic circuit for a Hall effect thruster*, 201.

[18] J. Navarro-Cavallé, M. Merino, E. Ahedo, M. Ruiz and V. Sánchez. *Design of Helicon Plasma Thruster susbsystems*, 2014.

[19] Elise F Morgan and Mary L Bouxsein. *Use of finite element analysis to assess bone strength*, 2005.

[20] Adriana Fernandez de Retana García. *Motor de plasma de efecto hall de 100 vatios*, UPM, 2004.

[21] Diego Escobar Antón and Alfredo Miguel Antón Sanchez *Desarrollo de un código híbrido PIC-fluido para simulación de motores de efecto Hall*

[22] Santiago Casado Perez. Design of a Helicon Plasma Thruster prototype.

[23] *Matlab web site* www.mathworks.com/store.

[24] Isidro Sánchez Álvarez Amortizacion y costes de préstamos con hojas de cálculo., 1990.